JOURNAL OF GEOPHYSICAL RESEARCH, VOL. 113, E12S33, doi:10.1029/2008JE003183, 2008

Spirit Mars Rover Mission to the Columbia Hills, Gusev Crater: Mission overview and selected results from the Cumberland Ridge to Home Plate

R. E. Arvidson,[1] S. W. Ruff,[2] R. V. Morris,[3] D. W. Ming,[3] L. S. Crumpler,[4] A. S. Yen,[5] S. W. Squyres,[6] R. J. Sullivan,[6] J. F. Bell III,[6] N. A. Cabrol,[7] B. C. Clark,[8] W. H. Farrand,[9] R. Gellert,[10] R. Greenberger,[1] J. A. Grant,[11] E. A. Guinness,[1] K. E. Herkenhoff,[12] J. A. Hurowitz,[5] J. R. Johnson,[12] G. Klingelhöfer,[13] K. W. Lewis,[14] R. Li,[15] T. J. McCoy,[16] J. Moersch,[17] H. Y. McSween,[17] S. L. Murchie,[18] M. Schmidt,[15] C. Schröder,[3] A. Wang,[1] S. Wiseman,[1] M. B. Madsen,[19] W. Goetz,[20] and S. M. McLennan[21]

Received 12 May 2008; revised 1 July 2008; accepted 31 July 2008; published 6 November 2008.

[1] This paper summarizes the Spirit rover operations in the Columbia Hills of Gusev Crater from sols 513 to 1476 and provides an overview of selected findings that focus on synergistic use of the Athena Payload and comparisons to orbital data. Results include discovery of outcrops (Voltaire) on Husband Hill that are interpreted to be altered impact melt deposits that incorporated local materials during emplacement. Evidence for extensive volcanic activity and aqueous alteration in the Inner Basin is also detailed, including discovery and characterization of accretionary lapilli and formation of sulfate, silica, and hematite-rich deposits. Use of Spirit's data to understand the range of spectral signatures observed over the Columbia Hills by the Mars Reconnaissance Orbiter's Compact Reconnaissance Imaging Spectrometer (CRISM) hyperspectral imager (0.4–4 μm) is summarized. We show that CRISM spectra are controlled by the proportion of ferric-rich dust to ferrous-bearing igneous minerals exposed in ripples and other wind-blown deposits. The evidence for aqueous alteration derived from Spirit's data is associated with outcrops that are too small to be detected from orbital observations or with materials exposed from the shallow subsurface during rover activities. Although orbital observations show many other locations on Mars with evidence for minerals formed or altered in an aqueous environment, Spirit's data imply that the older crust of Mars has been altered even more extensively than evident from orbital data. This result greatly increases the potential that the surface or shallow subsurface was once a habitable regime.

Citation: Arvidson, R. E., et al. (2008), Spirit Mars Rover Mission to the Columbia Hills, Gusev Crater: Mission overview and selected results from the Cumberland Ridge to Home Plate, *J. Geophys. Res.*, *113*, E12S33, doi:10.1029/2008JE003183.

1. Introduction

[2] The Mars Exploration Rover, Spirit, touched down on the volcanic plains of Gusev Crater on 4 January 2004. During its first 156 sols Spirit conducted traverses and made measurements on the olivine-bearing basaltic plains that

[1]Department of Earth and Planetary Sciences, Washington University, St. Louis, Missouri, USA.
[2]School of Earth and Space Exploration, Arizona State University, Tempe, Arizona, USA.
[3]Johnson Space Center, NASA, Houston, Texas, USA.
[4]New Mexico Museum of Natural History and Science, Albuquerque, New Mexico, USA.
[5]Jet Propulsion Laboratory, California Institute of Technology, Pasadena, California, USA.
[6]Department of Astronomy, Cornell University, Ithaca, New York, USA.
[7]NASA Ames/SETI Institute, Moffett Field, California, USA.
[8]Lockheed Martin Corporation, Littleton, Colorado, USA.
[9]Space Science Institute, Boulder, Colorado, USA.
[10]Department of Physics, University of Guelph, Guelph, Ontario, Canada.
[11]Center for Earth and Planetary Studies, National Air and Space Museum, Smithsonian Institution, Washington, District of Columbia, USA.
[12]U. S. Geological Survey, Flagstaff, Arizona, USA.
[13]Institut für Anorganische und Analytische Chemie, Johannes Gutenberg-Universität, Mainz, Germany.
[14]California Institute of Technology, Pasadena, California, USA.
[15]Department of Civil and Environmental Engineering and Geodetic Science, Ohio State University, Columbus, Ohio, USA.
[16]Department of Mineral Sciences, Smithsonian Institution, Washington, District of Columbia, USA.
[17]Department of Earth and Planetary Sciences, University of Tennessee, Knoxville, Tennessee, USA.
[18]Applied Physics Laboratory, Johns Hopkins University, Laurel, Maryland, USA.
[19]Niels Bohr Institute, University of Copenhagen, Copenhagen, Denmark.
[20]Max Planck Institute for Sonnensystemforschung, Katlenburg-Lindau, Germany.
[21]Department of Geosciences, State University of New York, Stony Brook, New York, USA.

0148-0227/08/2008JE003183$09.00

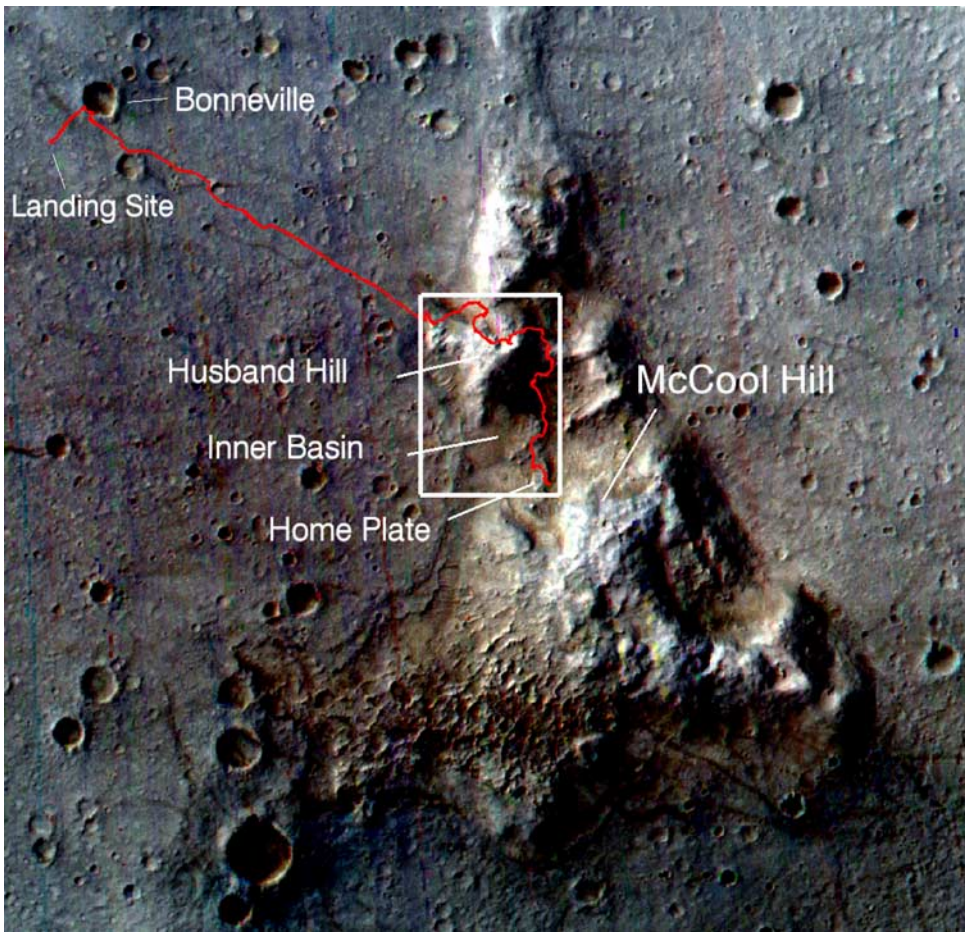

Figure 1. CRISM-based false color infrared composite for the Columbia Hills (~4.5 km wide at bottom margin) and surrounding cratered plains in Gusev Crater, with key features labeled. Spirit rover traverse locations from the landing site to the Low Ridge winter campaign site (where Spirit spent its second winter) located to the southeast of Home Plate are overlain as red line. Box denotes location for which a HiRISE image subset is shown in Figure 2. CRISM data with 18 m/pixel spatial from FRT00003192_07 using band 1098 nm for blue, 1518 for green, and 2528 nm for red are used in the composite. CTX image data with 6 m/pixel (frame PSP_001513_1654_XI_14S184W_061122) were used as the intensity in the color image to sharpen fine detail. North is to the top of this image. The striping is an artifact. Mars equirectangular projection.

dominate the floor of the Crater [*Arvidson et al.*, 2006a]. It then drove onto the older Columbia Hills and has been traversing and making measurements of the terrains, rocks, and soils within the Hills since then (Figures 1–3 and A1–A8, Table 2). Results for the mission that include analyses of plains and initial Columbia Hills data (including West Spur and a portion of Husband Hill, up to and including measurements on the float rock, Backstay, sol 512, on the Cumberland Ridge), were reported in numerous papers in two Journal of Geophysical Research 2006 Special Issues. In this paper, a mission narrative is provided for the period when the rover left Backstay until it parked on the northern flank of Home Plate (sol 1447) to wait out its third Martian winter and associated low solar energy conditions (Figure 3). Selected scientific results are presented in this paper that illustrate the synergistic use of the rover's Athena Science Payload (Table 1) [*Squyres et al.*, 2003] and that focus on understanding the geologic evolution of the Columbia Hills and implications for the role of water in modifying crustal materials. This paper complements papers that provide detailed findings about the geology, chemistry, and mineralogy of Husband Hill and the Inner Basin that are included in the third and fourth Journal of Geophysical Research Special Issues scheduled for publication in 2008.

[3] Since publication of the initial Journal of Geophysical Research MER Special Issues in 2006, the Mars Reconnaissance Orbiter (MRO) has begun operations and the Columbia Hills have been imaged with the Compact Reconnaissance Imaging Spectrometer for Mars (CRISM) [*Murchie et al.*, 2007], Context Imager (CTX) [*Malin et al.*, 2007] and High Resolution Imaging Science Experiment (HiRISE) instruments [*McEwen et al.*, 2007]. Analyses of selected MRO data are included in this paper to help define the regional-scale geomorphic and geologic contexts for Spirit's observations and to extend the type of information that can be derived from orbit down to the fine details that can be observed from a mobile surface platform.

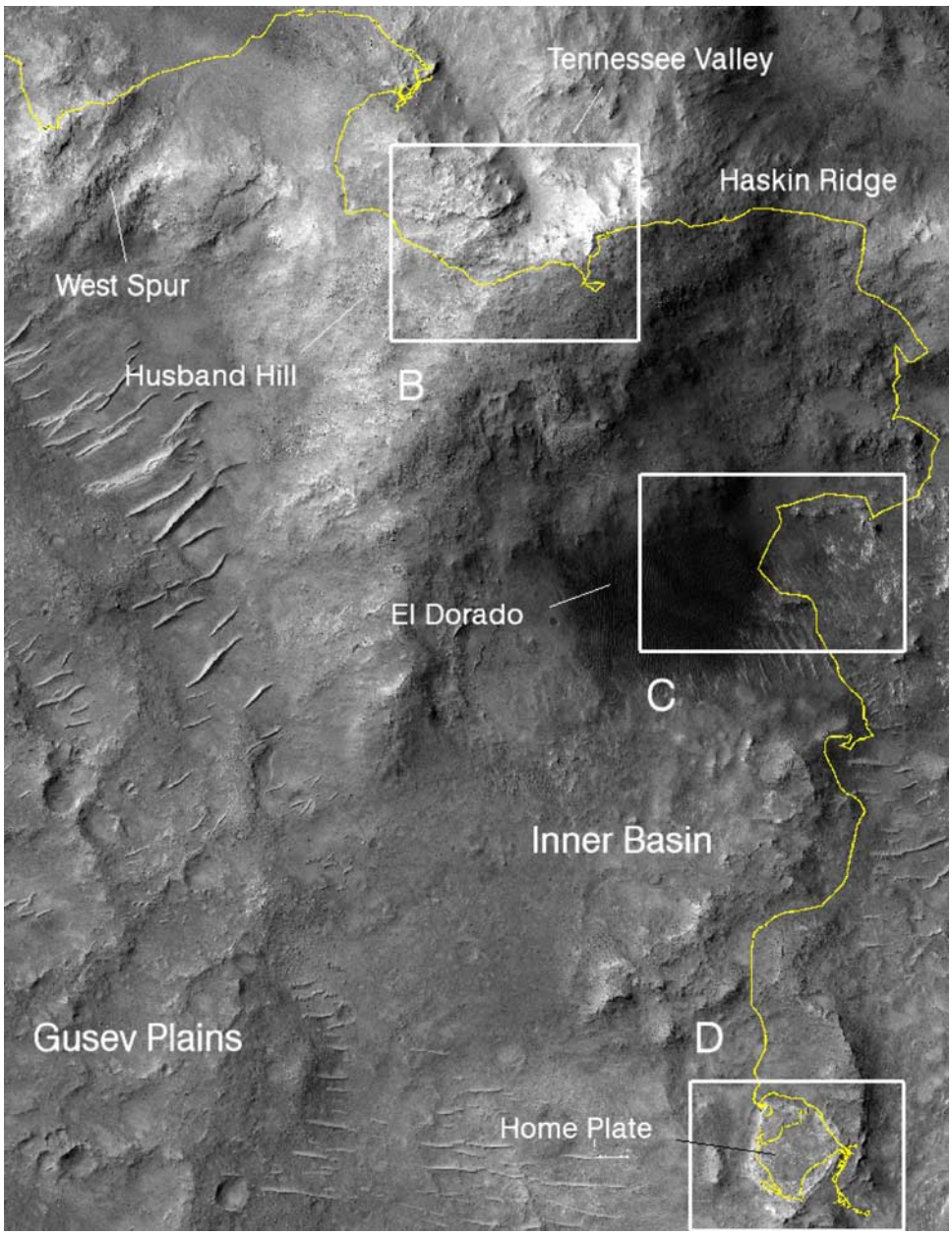

Figure 2a. HiRISE subframe covering Spirit's traverse and experiment sites (yellow line) in the Columbia Hills. Boxes show traverse regions examined in detail in subsequent Figures 2b–2d. Plan view generated using PSP_001513_1655_red image. Image covers ~1000 m in width.

Finally, implications for the extent of alteration of crustal materials on Mars by aqueous fluids are summarized on the basis of combined results from surface and orbital measurements for the Columbia Hills. Place names used in this paper are informal, with the exception of Meridiani Planum, Gusev Crater, and the Kau Desert.

2. Mission Narrative

[4] The operational approach for driving, approaching targets, and making measurements with Spirit (and Opportunity) and its Athena Payload (Table 1) has been detailed in previous papers [*Arvidson et al.*, 2006a; *Squyres et al.*, 2006] and will not be repeated here. Rather the focus is on a mission narrative, using the traverse locations overlain on MRO image data (Figures 1–2) to show the local and regional geomorphic context for the rover's observations. Table 2 provides a detailed summary of the traverse and measurement campaigns for Spirit for the period relevant to this paper, Figure 3 provides a graphical view of operations as a function of time with Martian southern hemisphere seasons delineated, and Appendix A provides a detailed set of traverse and experiment site maps superimposed onto a HiRISE-based map. As shown in Figures 1–2 and Appendix A, Spirit's traverses for the time period covered in this paper took place in the Columbia Hills, specifically Husband Hill and the Inner Basin. The Columbia Hills are a triangularly shaped complex of hills and intervening valleys that is embayed

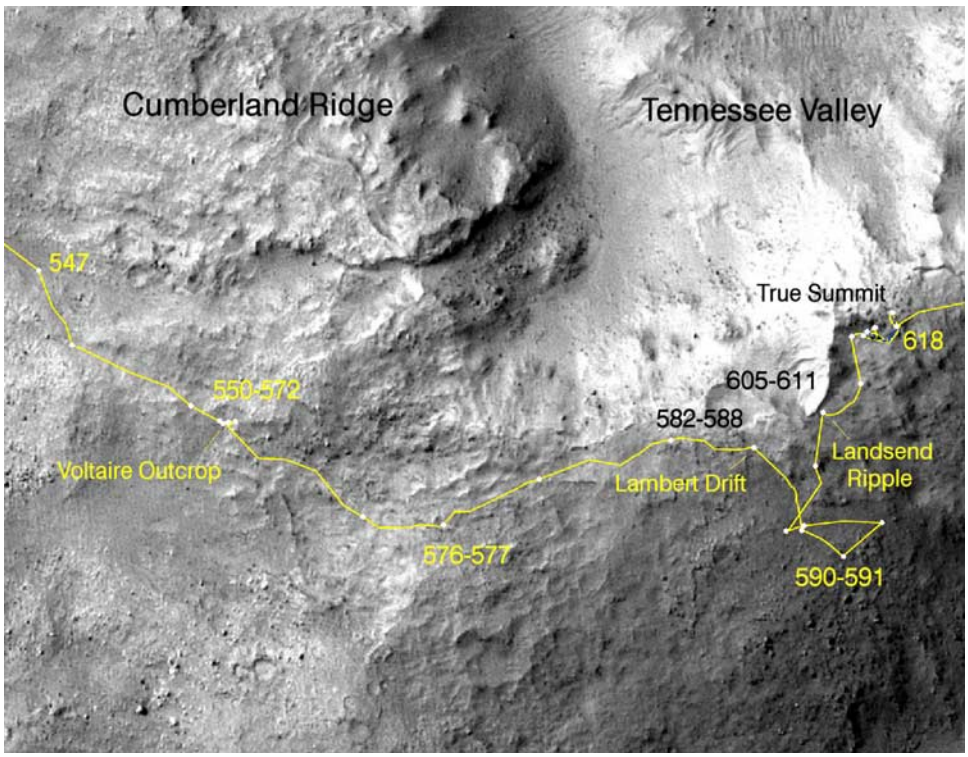

Figure 2b. HiRISE subframe covering the western and southwestern portions of Husband Hill and the Cumberland Ridge and a portion of the Tennessee Valley. Traverses are shown in yellow, along with locations for each sol.

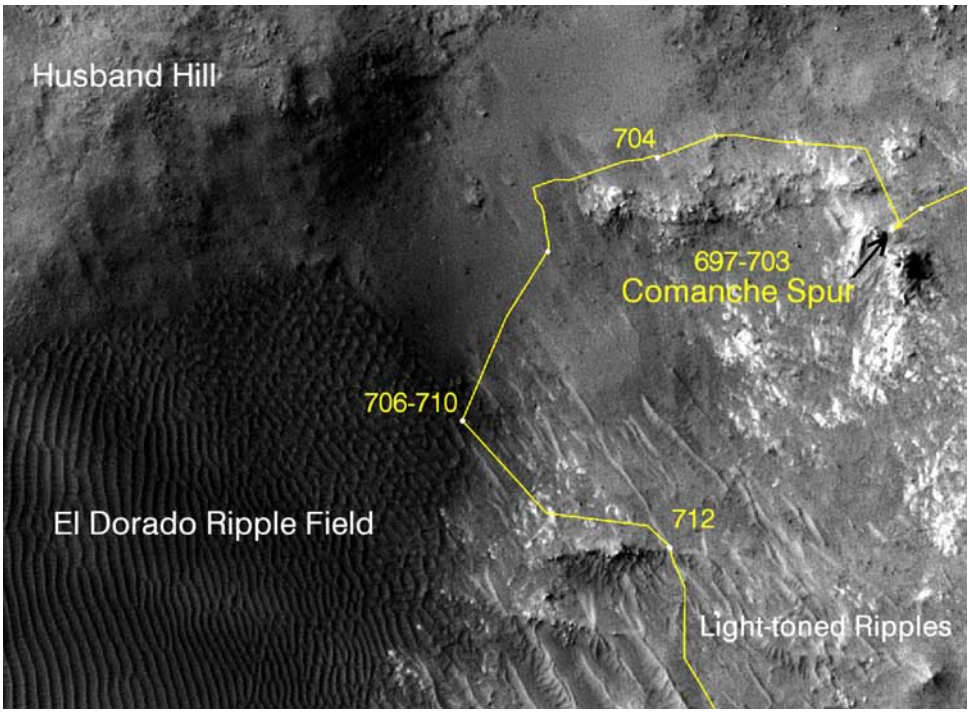

Figure 2c. HiRISE subframe covering a portion of the southern slope of Husband Hill, including the dark El Dorado ripple field, bright ripples extending to the southeast, and bright outcrops to the east and northeast of the El Dorado feature.

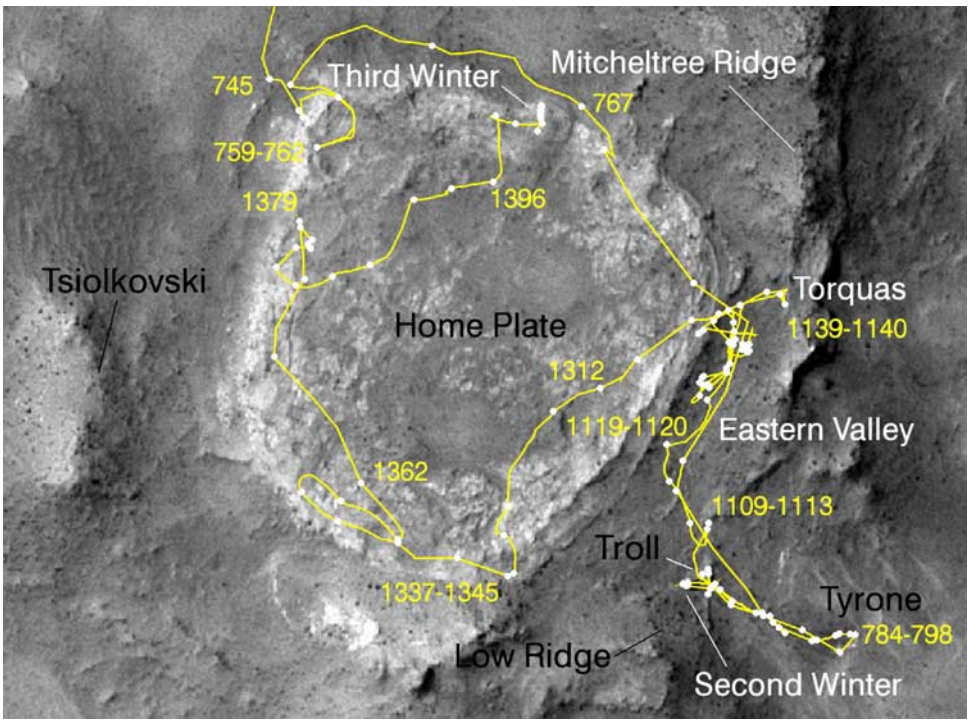

Figure 2d. HiRISE subframe covering the Inner Basin, centered on Home Plate. Key features are labeled. Second and third winters correspond to locations where Spirit parked for these periods.

by younger olivine-bearing volcanic plains [*McCoy et al.*, 2008]. From West Spur, where Spirit entered the Columbia Hills, the distance to the eastern boundary with the plains is ~1 km (Figure 1). Husband Hill, which was investigated in detail by Spirit, is ~0.5 km wide (E–W) and has a maximum elevation above the plains of ~80 m (Figures 2a–2c). The Inner Basin is located to the south of Husband Hill and the northwest of McCool Hill, and is dominated by a series of interconnected low hills that include Home Plate, an oval feature ~80 m wide that rises a few meters above the surrounding terrain (Figures 2a–2d). Mitcheltree Ridge and Low Ridge, oval to elongate hills that are located to the east and southeast of Home Plate, respectively, were also investigated by Spirit in some detail (Figures 2a–2d).

[5] Spirit left the basaltic float rock, Backstay, on sol 513 and continued its ascent to the summit of Husband Hill, traversing along the western slopes and cutting at low angles across topographic contours (to avoid excessive wheel slippage) to reach the western portion of the summit on sol 580. Immediately after leaving Backstay the outcrop Methuselah was examined using the payload instruments. The outcrop Independence was then examined in detail, including use of the right front wheel to scuff the bedrock and remove dust and coatings [*Clark et al.*, 2007]. Independence is a new rock type (relative to prior discoveries, [*Squyres et al.*, 2006]) characterized by the lowest FeO content (3.8% weight) of any rock measured on Mars [*Ming et al.*, 2008]. Spirit then encountered a suite of layered outcrops (Voltaire) and spent approximately 20 sols collecting in situ measurements for a series of targets on the outcrops while the remote sensing instruments observed dozens of targets within and beyond the outcrops (Table 3). The Voltaire experiments revealed a subclass of the Independence class of rocks (Assemblee) characterized by a high Cr_2O_3 content (2.9%) and a new class, Descartes, that is interpreted to be altered impact material (detailed in section 3 and by *Ming et al.* [2008]). The rover then continued its ascent to the top of Husband Hill, reached the summit and began a remote sensing campaign of the surrounding terrains from its high vantage point, including looking into the Inner Basin for safe paths for its descent to Home Plate. It then investigated an aeolian drift soil deposit (Lambert) before conducting observations on the float rock, Irvine, a subalkaline basalt rock class [*McSween et al.*, 2006; *Ming et al.*, 2008]. The Cliffhanger aeolian ripples at the head of the Tennessee Valley were then investigated, followed by the rock outcrop, Hillary (similar to the Watchtower rock class found on the northwestern slopes of Husband Hill [*Squyres et al.*, 2006; *Ming et al.*, 2008]), located on the eastern side of the summit.

[6] The next phase of the mission was the descent into the Inner Basin by way of Haskin Ridge (Figure 2b). The Kansas Outcrop was characterized (similar to Hillary [*Ming et al.*, 2008]), followed by a suite of measurements for olivine-rich outcrops (new Algonquin class rocks: Larry's Bench, Seminole, Algonquin, Comanche [*Morris et al.*, 2008; *Ming et al.*, 2008]) before approaching the dark ripple field, El Dorado, located on the southeastern slopes of Husband Hill. The rover traversed to the edge of the ripple field and conducted remote sensing and in situ measurements of these materials before continuing its drive to Home Plate. During one of its drives, after leaving El Dorado, Spirit encountered difficulty in reaching a waypoint because of wheel slippage. The wheels churned up shallow subsurface weakly bound rock or soil material that were found to

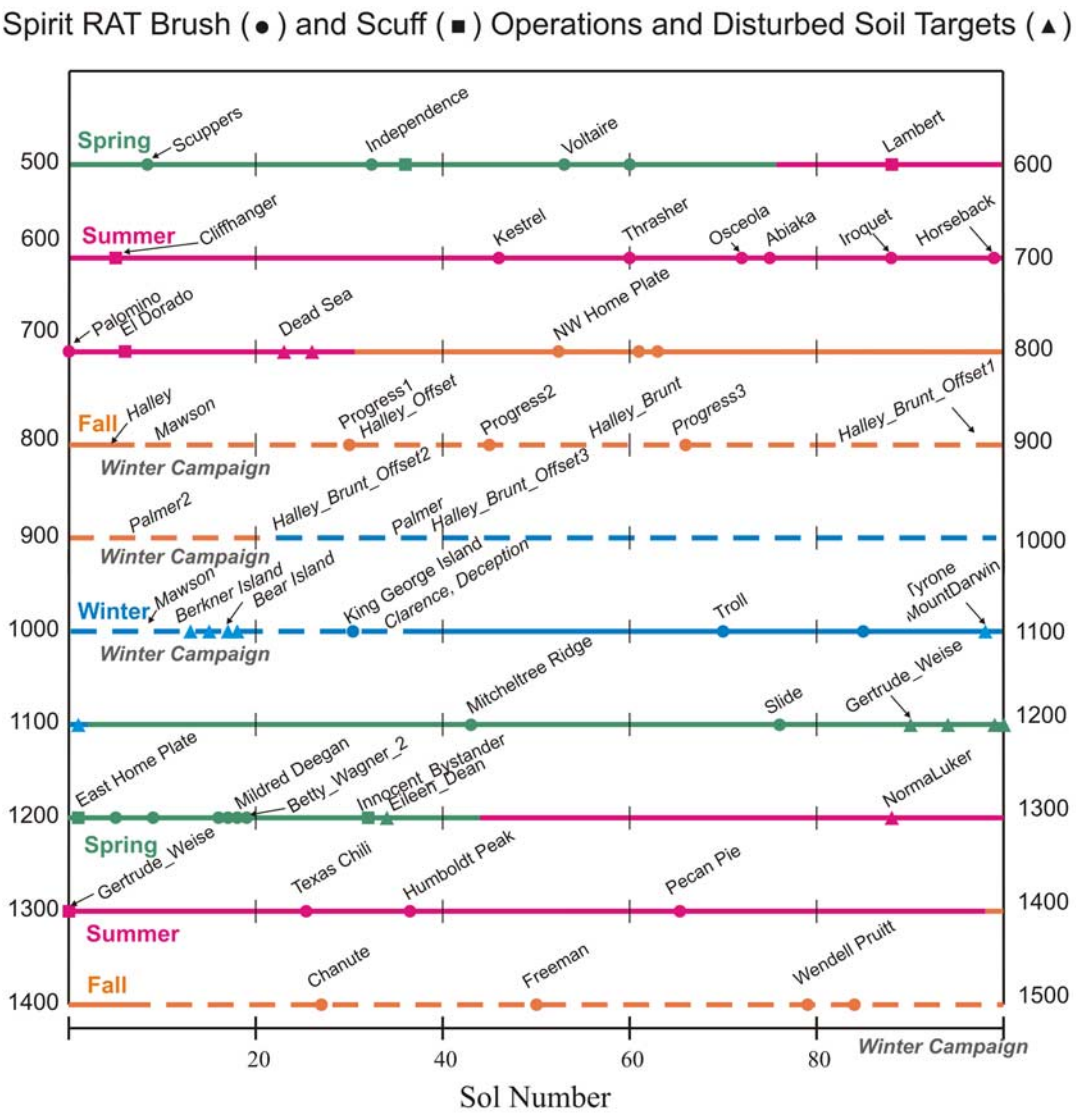

Figure 3. Spirit mission timeline from sol 500 to 1500. RAT brush operations are shown as circles (RAT grind was inoperative during the period shown), wheel-based scuffs to expose rock substrate (Independence) and soils are shown as squares, and soil targets exposed by wheel motions during drives are shown as triangles. Southern hemisphere seasons are shown in color coded form. Dashed lines show periods when Spirit spent its second and third winters. Italicized text indicates winter campaign activities that were not RAT brush, scuff, or disturbed experiments. This figure is meant to complement more detailed listings of activities provided in Table 2.

be enriched in hydrated ferric sulfate minerals (Arad deposits) [*Johnson et al.*, 2007; *Yen et al.*, 2008; *Wang et al.*, 2008]. Detailed measurements were made of these materials before the rover continued its drives toward Home Plate.

[7] Home Plate, a partially eroded volcaniclastic construct [*Squyres et al.*, 2007], was reached on sol 746 and a detailed measurement campaign was begun on the layered outcrop materials that showed fining upward sequences, along with extensive cross bedding (Barnhill, Posey (float), and Cool Papa Bell outcrops that define the Barnhill class of volcaniclastic rocks [*Ming et al.*, 2008]). A float rock, Fuzzy Smith, was encountered on the northeastern edge of Home Plate, and measurements showed it to be a new rock class highly enriched in silica, titanium, and perhaps iron sulfide minerals relative to other rock measurements by Spirit [*Squyres et al.*, 2007]. The rover then drove south through the Eastern Valley between the eastern edge of Home Plate and the western side of Mitcheltree Ridge. The intent was to head for the northern slopes of McCool Hill to find a suite of measurement locations for the rover to spend its second Mars winter. The need to park over the winter season was a consequence of the fact that Spirit is located at almost 15°S latitude and during the winter solstice the sun is directly overhead at 25°N latitude. Combined with accumulating dust on the solar panels, this situation called for a northerly vehicle tilt to maximize receipt of sunlight to maintain a reasonable battery charge. During its drive to McCool Hill, Spirit encountered another region with extensive wheel slippage associated with a gentle rise and terrace and excavated another high sulfate soil material (Tyrone). It

Table 1. Athena Payload and Engineering Camera Descriptions

Instrument	Key Parameters
	Mast Mounted
Panoramic Camera (Pancam)	Mulitspectral imager (0.4–1.0 μm) with stereoscopic capability; 0.28 mrad instantaneous field of view (IFOV); 16.8° × 16.8° field of view (FOV). Stereo baseline separation of 30 cm. External calibration target on rover deck.
Thermal Emission Spectrometer (Mini-TES)	Emission spectra (5–29 μm, 10 cm, 1 resolution) with 8 or 20 mrad FOV. Internal and external blackbody calibration targets.
	Instrument Deployment Device (IDD)-Mounted In Situ Package
Alpha Particle X-Ray Spectrometer (APXS)	^{244}Cm alpha particle sources, and X-ray detectors, 3.8 cm FOV.
Mössbauer Spectrometer (MB)	^{57}Fe spectrometer in backscatter mode; Co/Rh source and Si-PIN diode detectors; field of view approximately 1.5 cm^2.
Microscopic Imager (MI)	30 μm/pixel monochromatic imager (1024 × 1024) with 6 mm depth of field.
Rock Abrasion Tool (RAT)	Tool capable of brushing or abrading 5 mm deep by 4.5 cm wide surface on rocks.
	Magnets
Filter	Located at front of rover within Pancam FOV. Weak magnet to cull suspended particles from atmosphere and examined by Pancam, MI, APXS, and MB.
Capture	Located at front of rover within Pancam FOV next to filter magnet. Strong magnet to cull suspended particles from atmosphere. Examined by Pancam, MI, APXS, and MB.
Sweep	Located next to Pancam calibration target. Intended to separate magnetic from nonmagnetic particles. Examined by Pancam.
RAT	Four magnets of different strengths built into RAT. Examined by Pancam and Hazcam when IDD points RAT toward cameras.
	Engineering Cameras
Navigation Cameras (Navcam)	Mast-mounted panchromatic stereoscopic imaging system with 0.77 mrad IFOV; 45° FOV, and 20 cm stereo baseline separation. For planning sequences.
Hazard Avoidance Cameras (Hazcam)	Front and rear-looking panchromatic stereoscopic imaging systems with 2 mrad IFOV; 123° FOV, 10 cm stereo baseline separation. For path planning and hazard avoidance during traverses.

became clear that traversing to McCool Hill would be difficult indeed, particularly when it became evident that the front right wheel drive motor had failed. Thus the decision was made to drive expeditiously to a nearby north-facing slope to spend the winter. The vehicle was commanded to drive to the northeast slope of Low Ridge and achieved an 8° northerly tilt, a value sufficient to survive its second winter season.

[8] Spirit spent sols 805 to 1037 at the Low Ridge site during its winter campaign phase and conducted a suite of experiments focused on long duration Alpha Particle X-Ray Spectrometer (APXS) and Mössbauer Spectrometer (MB) observations of soils and rocks within the Instrument Deployment Device (IDD) work volume, acquisition of a 13 filter high fidelity ''McMurdo Panorama'' using the Pancam imaging system (see Table 1 for instrument descriptions), photometry studies, monitoring surface and atmospheric targets for temporal changes using the various imaging systems (Table 1), and obtaining hundreds of emission spectra of the atmosphere and surface using the Mini-Thermal Emission Spectrometer (Mini-TES). The rock experiments included multiple in situ measurements of the platy buff-colored outcrops typified by Halley (rock class characterized by enrichment in hematite relative to other rocks [*Morris et al.*, 2008; *Ming et al.*, 2008]) and an attempt to use the Rock Abrasion Tool (RAT) brush to progressively bore into deeper and deeper soil horizons with measurements made at each horizon (Progress soil experiments). The inoperative right front wheel was dragged from Tyrone back to the winter campaign site as the rover drove backward. In a serendipitous turn of events, sulfate-rich Tyrone soil deposits excavated while the vehicle was in the Tyrone area were caught within the right front wheel cowling and released along the ~40 m drive to Low Ridge, including deposits within the winter campaign work volume. Long duration measurements were made on these materials (Berkner Island). Finally, long duration magnet measurements were also made during the winter campaign [*Madsen et al.*, 2008].

[9] Leaving the winter campaign site was done with care toward the end of the winter season, first with a short bump to finely layered granular outcrops within Low Ridge (Graham Land, King George Island target) and then to a vesicular basalt float rock (Esperanza) also located on Low Ridge. The Esperanza measurements were cut short because of rising atmospheric dust opacity and thus decreasing solar energy on the panels. Spirit was sent on a short drive to a more northerly tilted terrain that also placed the vehicle for in situ measurements on the Troll outcrops (Montalva and Riquelme targets, a new rock class defined by high hematite and K_2O contents [*Morris et al.*, 2008; *Ming et al.*, 2008]). Next Spirit was directed to drive back to within 10 m of the Tyrone disturbed soil deposits to acquire remote sensing and in situ data to further characterize the deposits and to search

Table 2. Major Activities for Spirit Organized by Sol[a]

Earth Date	Sols	Description of Activities	Site at Start of Sol
13–14 Jun. 2005	513–514	Drive and "Methuselah" Outcrop targeted RS	110
15–27 Jun. 2005	515–527	Drive toward summit of "Husband Hill"; RS	111–112
28 Jun. to 5 Jul. 2005	528–535	"Independence" Outcrop: approach, IDD: "Franklin," "Jefferson," and other targets; RS	112
6–13 Jul. 2005	536–543	Independence Outcrop: scuff, IDD, and RS "Penn" target; "Independence Panorama"	112
14–20 Jul. 2005	544–549	Drive toward summit of Husband Hill; RS	112
21–27 Jul. 2005	550–556	"Voltaire": "Descartes" Outcrop: approach, IDD, and RS "Discourse" target	113
27 Jul. to 2 Aug. 2005	556–562	Voltaire: "Bourgeoisie" Outcrop: bump, IDD, and RS "Chic," "Gentil_Matrice," and other targets	113
2–4 Aug. 2005	562–564	Voltaire: Haussmann Outcrop: bump, IDD, and RS "Rue_Legendre," "Rue_Laplace," and "Sophie_Germain"	113
5–12 Aug. 2005	565–572	Voltaire: "Assemblee" Outcrop: bBump, IDD, and RS "Gruyere" targets	113
13–23 Aug. 2005	573–582	Drive toward summit of Husband Hill; RS	113
23–25 Aug. 2005	582–584	Husband Hill Summit Panorama	114
25–29 Aug. 2005	584–588	"Lambert" soil: IDD and RS "Couzy" and "Whymper" targets	114
30–31 Aug. 2005	589–590	Drive toward "Inner Basin Overlook #1"; RS	114
1–2 Sep. 2005	591–592	Drive toward "Inner Basin Overlook #2"; RS	114
3 Sep. 2005 to 7 Sep. 2007	593–597	Magnet science; RS	114
8–12 Sep. 2005	598–602	Approach, IDD, and RS "Irvine" float target	114
13–21 Sep. 2005	603–611	"Cliffhanger" ripple: approach, scuff, IDD, and RS "Landsend" and "Hang2" targets, photometry campaign	114
22 Sep. to 4 Oct. 2005	612–623	Drive toward true summit of Husband Hill; RS; "Everest Panorama"	114
5–15 Oct. 2005	624–634	"Hillary" Outcrop: approach, IDD, and RS "Khumjung" and "NamcheBazaar" targets	114
16–22 Oct. 2005	635–641	Drive toward "Haskin Upper Ridge"; RS	114–118
23–29 Oct. 2005	642–648	"Kansas" Outcrop: approach, IDD, and RS "Kestral" target	118
25 Oct. 2005 to 26 Oct. 2006	644–645	Anomaly precludes science activities	–
30 Oct. to 1 Nov. 2005	649–651	Drive toward Haskin Upper Ridge; RS	118
2–5 Nov. 2005	652–654	Remote sensing	118
6 Nov. 2005	655	Drive onto "Haskin Lower Ridge"	118
7–8 Nov. 2005	656–657	Remote sensing	119
9 Nov. 2005	658	Drive south toward "Waypoint"; RS	119
10–14 Nov. 2005	659–663	"Larry's Bench" Outcrop: approach, IDD, and RS "Thrasher" target	119
15–20 Nov. 2005	664–669	Drive south toward "Waypoint"; RS	119
21–28 Nov. 2005	670–677	"Seminole" Outcrop: approach, IDD, and RS "Osceola" and "Abiaka" targets; "Seminole Panorama"	119
29 Nov. to7 Dec. 2005	678–686	Drive toward "Algonquin" Outcrop; RS	119
8–10 Dec. 2005	687–689	Algonquin Outcrop IDD and RS "Iroquet" target	119
12–18 Dec. 2005	690–696	Drive toward "Comanche Spur" Outcrop; RS	119–120
19–25 Dec. 2005	697–703	Comanche Spur Outcrop: approach, IDD, and RS "Horseback," and "Palomino" targets	120
26–27 Dec. 2005	704–705	Drive toward "El Dorado" ripple; RS	120
28 Dec. to 1 Jan. 2006	706–710	El Dorado ripple: approach, scuff, IDD, and RS "Gallant Knight," "Edgar," and "Shadow" targets, photometry campaign	120–121
2–10 Jan. 2006	711–719	Drive toward "Home Plate"; RS	121–122
11–13 Jan. 2006	720–722	Remote sensing	122
14–16 Jan. 2006	723–725	"Arad" disturbed soil: IDD and RS "Samra" and other targets	122
17–27 Jan. 2006	726–735	Drive toward Home Plate; RS	122–123
25–27 Jan. 2006	733–735	Dynamic brake anomaly and diagnostics	–
28–29 Jan. 2006	736–737	"BuZhou" and "Pan_Gu" float targets: IDD and RS	123
30 Jan. to 5 Feb. 2006	738–744	Drive toward Home Plate; RS	123
6 Feb. 2006	745	Remote sensing	124
7–11 Feb. 2006	746–750	"Barnhill" Outcrop: approach, IDD, and RS "Ace," "Pitcher," and "Fastball" targets	124
12–15 Feb. 2006	751–754	"Posey" Outcrop: approach, IDD, and RS "Manager" target	124
16 Feb. 2006	755	Drive toward Home Plate; RS	124
17–19 Feb. 2006	756–758	Remote sensing	124

Table 2. (continued)

Earth Date	Sols	Description of Activities	Site at Start of Sol
20–25 Feb. 2006	759–763	"Cool_Papa_Bell" Outcrop: approach, IDD, RS "Stars," and "Crawfords" targets	124
26 Feb. to 1 Mar. 2006	764–767	Drive around Home Plate Rim; RS	124–125
2–5 Mar. 2006	768–771	"Fuzzy Smith" float: approach, IDD, and RS	125
6 Mar. to 5 Apr. 2006	772–801	Drive toward "McCool Hill"; RS	125–126
13–15 Mar. 2006	779–781	Right front drive actuator fault and diagnostics	–
21 Mar. 2006	787	Right front wheel declared nonoperational	–
18 Mar., 24– 25 Mar., and 1 Apr. 2006	784, 790–791, 798	RS "Tyrone" disturbed soil	126
6–9 Apr. 2006	802–805	Drive toward and approach "Low Ridge" location for winter campaign experiments; RS	126
10–12 Apr. 2006	806–808	Remote sensing	126–127
13–15 Apr. 2006	809–811	"Enderbyland" IDD: "Halley" Outcrop target	127
16–22 Apr. 2006	812–818	Enderbyland IDD: "Mawson" soil target; Begin McMurdo Panorama	127
22 Apr. 2006	818	RS Tyrone disturbed soil	127
23–25 Apr. 2006	819–821	Remote sensing	127
26 Apr. to 3 May 2006	822–829	Enderbyland IDD and RS "Progress" soil target	127
30 Apr. 2006	826	RS "Tyrone" disturbed soil	127
4–5 May 2006	830–831	Enderbyland IDD and RS "Progress1" target	127
6–13 May 2006	832–838	Enderbyland IDD: "Halley_Offset" Outcrop target	127
14–16 May 2006	839–841	Enderbyland IDD: Progress1 brushed soil target	127
17 May 2006	842	IDD positioning test; RS	127
18–19 May 2006	843–844	Remote sensing	127
20–29 May 2006	845–854	Enderbyland: IDD and RS "Progress2" brushed soil target	127
24–26 May 2006	850–851	Anomaly precludes science activities	–
30 May to 4 Jun. 2006	855–860	Remote Sensing	127–128
4 Jun. 2006	860	Navcam photon transfer calibration experiment	128
5 Jun. 2006	861	Enderbyland IDD: "Halley_Brunt" Outcrop target	128
6–8 Jun. 2006	862–864	Remote sensing	128
8 Jun. 2006	864	RS Tyrone disturbed soil target	128
9 Jun. 2006	865	Rear Hazcam photon transfer calibration experiment	128
10–14 Jun. 2006	866–870	Enderbyland IDD: "Progress3" brushed soil target	128
12 Jun. 2006	868	Front Hazcam photon transfer calibration experiment	128
15–19 Jun. 2006	871–874	Remote sensing	128
20 Jun. to 4 Jul. 2006	875–889	Enderbyland IDD: Halley_Brunt Outcrop target	128
21 Jun. 2006	876	Microscopic Imager photon transfer calibration experiment	128
27 Jun. 2006	882	Left Pancam photon transfer calibration experiment	128
29 Jun. 2006	884	Right Pancam photon transfer calibration experiment	128
5 Jul. 2006	890	Mini-TES elevation actuator calibration	128
6 Jul. 2006	891	Remote sensing	128
7 Jul. 2006	892	Flight software uplink	128
8 Jul. 2006	893	RAT calibration; RS	128
9–11 Jul. 2006	894–896	Remote sensing	128
12–19 Jul. 2006	897–904	Enderbyland IDD: "Halley_Brunt_Offset1" Outcrop target	128
19 Jul. 2006	904	RAT unjamming activity	128
20–21 Jul. 2006	905–906	Remote sensing	128
22 Jul. 2006	907	Flight software build; RS	128
24 Jul. 2006	908	Enderbyland IDD: "Palmer" ripple target	128
25 Jul. 2006	909	Remote sensing	128
26 Jul. 2006	910	RAT cleaning and calibration; RS	128
27–28 Jul. 2006	911–912	Remote sensing	128
29 Jul. 2006	913	Enderbyland IDD: "Palmer2" ripple target	128
30 Jul. to 4 Aug. 2006	914–919	Remote sensing; complete McMurdo Panorama	128
5 Aug. 2006	920	Microscopic Imager photon transfer calibration experiment; RS	128
6–11 Aug. 2006	921–926	Remote Ssensing; begin filling-in McMurdo Panorama holes	128
7 Aug. 2006	922	RS Tyrone disturbed soil	128
12–14 Aug. 2006	927–929	Enderbyland IDD: "Halley_Brunt_Offset2" target	128
15–21 Aug. 2006	930–936	Remote sensing, including photometry campaign	128
16 Aug. 2006	931	Complete filling-in McMurdo Panorama holes	128
19 Aug. 2006	934	Begin McMurdo Deck Panorama	128

Table 2. (continued)

Earth Date	Sols	Description of Activities	Site at Start of Sol
22 Aug. 2006	937	Enderbyland IDD: Palmer target	128
23/06–26 Aug. 2006	938–941	Remote sensing	128
27 Aug. to 3 Sep. 2006	942–948	Enderbyland IDD: "Halley_Brunt_Offset3" target	128
31 Aug. to 1 Sep. 2006	945–946	Anomaly precludes science observations	–
4–9 Sep. 2006	949–954	Remote sensing	128
10–24 Sep. 2006	955–969	IDD capture and filter magnets; RS	128
14 Sep. 2006	959	RS Tyrone disturbed soil	128
17 Sep. 2006	962	Finish McMurdo Deck Panorama	128
20–22 Sep. 2006	965–967	Flight software boot and diagnostics	–
25 Sep. to 31 Oct. 2006	970–1005	MB filter magnet study; RS	128
25 Sep. and 8 Oct. 2006	970, 982	RS Tyrone disturbed soil	128
17–131 Oct. 2006	991–1005	Solar conjunction	–
18, 23, and 31 Oct. 2006	992, 997, 1005	RS Tyrone disturbed soil	128
1 Nov. 2006	1006	IDD capture and filter magnets; RS Tyrone disturbed soil	128
2–3 Nov. 2006	1007–1008	IDD and RS rock clast targets; IDD Mawson target	128
4–7 Nov. 2006	1009–1012	Remote sensing	128
5 Nov. 2006	1010	Bump bright soil tracks; RS	128
8–11 Nov. 2006	1013–1016	IDD: "Berkner_Island_1" disturbed soil target	128
12–17 Nov. 2006	1017–1021	IDD: "Bear_Island" disturbed soil target	128
17 Nov. 2006	1021	Pancam calibration target photometry experiment	128
18 Nov. 2006	1022	Bump layered outcrop; RS	128
19–22 Nov. 2006	1023–1026	Remote sensing	128
23–31 Nov. 2006	1027–1035	"Graham_Land" Outcrop: IDD and RS "King_George_Island" target	128
30 Nov. 2006	1034	IDD "Clarence" and "Deception" targets	128
1 Dec. 2006	1036	RS Tyrone disturbed soil; RS	128
3–18 Dec. 2006	1037–1052	Drive toward "Esperanza" float; RS	128
13 Dec. 2006	1047	RS Tyrone disturbed soil	128
20–28 Dec. 2006	1053–1061	IDD and RS "Palma" target on Esperanza float	128
28 Dec. 2006	1061	RS Tyrone disturbed soil	128
29 Dec. 2006	1062	Drive to location where solar arrays face sun	128
30 Dec. 2006 to 4 Jan. 2007	1063–1068	Atmospheric RS	128
5–25 Jan. 2007	1069–1089	"Troll" Outcrop: approach, IDD and RS "Montalva" target	128
16–28 Jan. 2007	1080–1091	Troll Outcrop: RS and IDD "Riquelme" and "Zucchelli" targets	128
21 Jan. 2007	1085	RS "Contact" and "Londonderry" targets	128
22 Jan. 2007	1086	IDD "Svea" and "Maudhem" targets	128
29 Jan. to 9 Feb. 2007	1092–1103	Drive toward Tyrone; IDD and RS "Mount Darwin" target	128
9 Feb. 2007	1103	Drive toward Troll	128
10 Feb. 2007	1104–1106	Automode	128
13–19 Feb. 2007	1107–1113	Approach and RS "Bellingshausen," and "Fabien" and other outcrops	128
20 Feb. to 10 Mar. 2007	1114–1131	Drive toward Home Plate; IDD and RS; atmospheric RS	128
11–26 Mar. 2007	1132–1147	Approach, IDD, and RS "Mitcheltree Ridge" Outcrop: "Torquas" target	128
16 Mar. 2007	1137	MRO safe mode, run-out science submaster executed, photometry measurements	128
27–28 Mar. 2007	1148–1149	Drive toward Home Plate	128
29 Mar. to 20 Apr. 2007	1150–1171	Drive toward "Madeline English" Outcrop; IDD and RS	128–129
1–8 Apr. 2007	1153–1160	IDD and RS "Elizabeth Mahon" target	128
21–30 Apr. 2007	1172–1181	RS and IDD "Everett," "Slide," and "Good Question" Outcrop targets	129
1–2 May 2007	1182–1183	RS "Gertrude_Weise" disturbed soil	129
3–4 May 2007	1184–1185	Drive toward, IDD, and RS Gertrude Weise	129
5–24 May 2007	1186–1204	IDD "Kenosha Comets," and "Lefty Ganote" targets	129
24 May 2007	1204	RS El Dorado ripples	129
25 May to 3 Jun. 2007	1205–1214	RS and IDD"Home Plate Outcrop" "Pesapallo," "Superpesis," and "June_Emerson" targets	129
4–9 Jun. 2007	1215–1220	Approach, RS, and IDD Home Plate Outcrop "Elizabeth Emery," "Jane Stoll," "Mildred Deegan," and "Betty Wagner's Daughter" targets	129
10 Jun. 2006 to 23 Jun. 2007	1221–1234	Approach, IDD, and RS "Nancy Warren" Outcrop and target	129–130
13 Jun., 22 Jun., and 12 Jul. 2007	1224, 1233, 1252	Dust cleaning events	130
23 Jun. to 6 Jul. 2007	1234–1246	IDD and RS "Eileen Dean" disturbed soil; atmospheric RS	130
30 Jun. to 3 Jul. 2007	1240–1243	Stand down; atmospheric RS	130

Table 2. (continued)

Earth Date	Sols	Description of Activities	Site at Start of Sol
7 Jul. to 21 Aug. 2007	1247–1291	Nancy Warren Outcrop IDD "Innocent Bystander" and "Norma Luker "targets; RS, including photometry campaign	130
9–20 Aug. 2007	1279–1290	MI diagnostics	130
22 Aug. to 3 Sep. 2007	1292–1304	RS and drive toward Home Plate Mini-TES recalibration using "Gertrude Weise" disturbed soil	130
4–7 Sep. 2007	1305–1308	Drive toward Home Plate	130
7 Sep. 2007	1308	Reach Home Plate, RS	130
9–10 Sep. 2007	1309–1310	RS Home Plate	130
10–14 Sep. 2007	1310–1314	Drive toward Home Plate Site 2; RS	130–131
15 Sep. to 7 Oct. 2007	1315–1337	Drive toward Home Plate Site 3; RS; "Home Plate South Panorama"	131
25–30 Sep. 2007	1325–1330	IDD "Texas Chili" Outcrop target	131
16 Oct. 2007	1337–1345	Home Plate Site 3a feature: IDD "Humboldt Peak" float target	131
17–23 Oct. 2007	1346–1352	Drive toward Home Plate Site 4; RS	131
17 and 26–31 Oct. 2007	1346, 1355–1360	RAT diagnostics; RS	131–132
19–23 Oct. 2007	1348–1352	Long-baseline stereo off "Home Plate"	131
24–25 Oct. 2007	1353–1354	Drive toward Home Plate south off-ramp; RS	131
1–3 Nov. 2007	1361–1363	Drive toward Home Plate Site 5; RS	132
4–10 Nov. 2007	1364–1370	IDD "Pecan Pie" Outcrop target; RS	132
11–14 Nov. 2007	1371–1374	Drive toward Home Plate Site 6	132
15–20 Nov. 2007	1375–1380	Drive toward Home Plate Site 7; RS	132
20 Nov. to 19 Dec. 2007	1380–1408	Drive toward winter campaign site; atmospheric RS	132–133
20 Dec. to 15 Jan. 2008	1409–1434	IDD "Chanute" Outcrop target; Tuskegee Panorama	133
16–20 Jan. 2008	1435–1439	RS Fuzzy Smith float; atmospheric RS; RAT imaging	133
21 Jan. to 23 Mar. 2008	1440–1500	Atmospheric RS	133–134
26 Jan. to 6 Feb. 2008	1445–1456	IDD "Freeman" Outcrop target; RS "Fuzzy Smith 2 Float," "Winston Gaskins 2" Outcrop target	133
26 Feb. 2006 to 20 Mar. 2008	1475–1497	IDD and RS "Wendell Pruitt" Outcrop and "Arthur C. Harmon" Soil targets; RS "C.S. Lewis" and Freeman Outcrop targets	134
27 Feb. 2008	1476	Begin Bonestell Panorama	134

[a]Measurements were made on rock outcrops, float rocks, soils, and soils disturbed by the vehicle's wheels. RS, remote sensing; IDD, Instrument Deployment Device. Note that the Mini-TES instrument capabilities were affected by dust on the mirror on sol 420, followed by additional accumulation during the course of the extended mission. Other acronyms defined in Table 1.

for changes relative to measurements done before arriving at Low Ridge for the winter. After finishing these measurements, the rover focused on remote sensing and in situ work on the finely layered outcrops on the western side of Mitcheltree Ridge, most notably Torquas (rock class defined by high K_2O, Zn, Ni contents and enrichment in magnetite [*Morris et al.*, 2008; *Ming et al.*, 2008]). Spirit was then commanded to approach and make remote sensing and in situ measurements on outcrops just to the east of Home Plate, including Elizabeth Mahon (new class of rock characterized by high SiO_2 content [*Squyres et al.*, 2008; *Ming et al.*, 2008]), Madeline English, Everett and Good Question (latter two rocks define new classes on the basis of high MgO and magnetite contents for the former, and high SiO_2 and low MnO contents for the latter [*Morris et al.*, 2008; *Ming et al.*, 2008]). During one of its backward drives Spirit's right front wheel excavated light-toned soil deposits (Gertrude Weise), which Mini-TES indicated and APXS measurements later confirmed have extraordinarily high silica contents [*Squyres et al.*, 2008]. After completing measurements on these unusual deposits the rover drove to acquire detailed remote sensing and in situ measurements of the strata exposed on the eastern flank of Home Plate on sols 1205 to 1220 (Pesapallo, Superpesis, June Emerson, Elizabeth Emery). An outcrop identified as silica-rich from Mini-TES observations was then examined (Nancy Warren), followed by another bright deposit excavated by the right front wheel (Eileen Dean). The vehicle was then commanded to drive over and crush rocks adjacent to Nancy Warren and broke open and obtained in situ observations on the silica-rich targets Innocent Bystander and Norma Luker.

[10] During an approximately 60 sol period when the vehicle was parked over Innocent Bystander waiting out the low solar energy conditions associated with a southern hemisphere dust storm, one or more of the Mini-TES mirrors was significantly contaminated by dust, reducing the spectral sensitivity of this instrument. After the dust storm, Spirit was commanded to approach and ascend onto Home Plate and obtain measurements designed to characterize the rocks on the top of Home Plate and rocks on the South Promontory. With the third winter season approaching, an increasing cover of dust on the solar panels, and hindered mobility on slopes due to the inoperative right front wheel, a decision was made to drive to the northern flank of Home Plate to achieve a maximum possible

Table 3. Summary of the Voltaire Outcrop Measurement Campaign

Sols	Description of Activities
552	Started IDD work on Discourse target located on Descartes Outcrop with a MI mosaic and APXS integration.
553	Brush, MI, and APXS on Discourse.
554–555	MB integration on Discourse.
556	MI on two additional Descartes targets: Petitchou and Moncherie (dark clast). At end of sol the rover turned to face the rocks Sourir, Bourgeoisie, and Haussmann.
557	Started IDD work on Bourgeoisie Outcrop, with three MI mosaics and an APXS integration. Targets Gallant, Gentil, and Chic (APXS target), clast embedded in the outcrop.
558–559	MB integration on Chic target (Bourgeoisie)
560	Acquired MI, RAT brush, MI, and APXS data on Gentil Matrice target (Bourgeoisie).
561	MB integration on Gentil Matrice target.
562	Short MB integration on Gentil Matrice target. Sol finished with the rover turning to face Haussmann.
563	Three MI mosaics acquired on Haussmann Outcrop for targets Rue Legendre, Rue Sophie Germain, and Rue Laplace. An APXS measurement acquired on Rue Laplace.
564	Sol activities were lost when uplink did not make it to the rover.
565	Short drive to Assemblee.
566	MI and APXS integration on Gruyere target (Assemblee Outcrop). Target was too rough for RAT brush.
567–570	Four sols of MB integration on Gruyere target because of low Fe content.
571	MI and APXS integration on second Gruyere target to test whether clasts were source of high Cr in initial APXS measurement. Target name Gruyere_APXS.
572	IDD stowed in preparation of driving.
573	Drove away from Voltaire outcrops, looking back with Pancam during middrive.

northerly tilt to survive the winter season. Spirit reached the site on sol 1408 and began a set of maneuvers to bump down the flank to follow the sun as it moved north toward its solstice position. Remote sensing and in situ measurements continued to be made as the vehicle moved downslope, contingent upon available power.

3. Husband Hill: Voltaire Outcrop Campaign

[11] The first scientific highlight to be discussed is the discovery of the layered Voltaire outcrops encountered after Spirit left the Independence Outcrop and continued its ascent to the summit of Husband Hill (Figure 2b and Table 3) [also see *Clark et al.*, 2007]. Outcrops observed prior to discovery of the Voltaire sequence showed that bedding was largely conformable with the topography of the Hills, including outcrops on West Spur and the ensemble of outcrops found in Larry's Lookout on the northwest flank of Husband Hill (Appendix A) [*Squyres et al.*, 2006]. The observation that the outcrop pattern on Husband Hill conforms to topography implies that the Hill is the geomorphic expression of an antiformal structure and that Spirit has largely examined the top of the section [*McCoy et al.*, 2008]. On the other hand, the end-of-drive Pancam mosaic acquired on sol 549 showed a set of strata approximately 5 m long in a NE–SW direction and 2.5 m wide in a NW-SE direction, with a dip to the SE, i.e., dipping into the hill (Figure 4). The orientation of the strata was verified using a CAVE Virtual Reality Immersion System to view the outcrops at full scale and in three dimensions using Pancam and Navcam mosaics. This outcrop, which was named Voltaire because it was discovered on Bastille Day (14 July 2005), is truncated to the SW by a shallow trough and to the

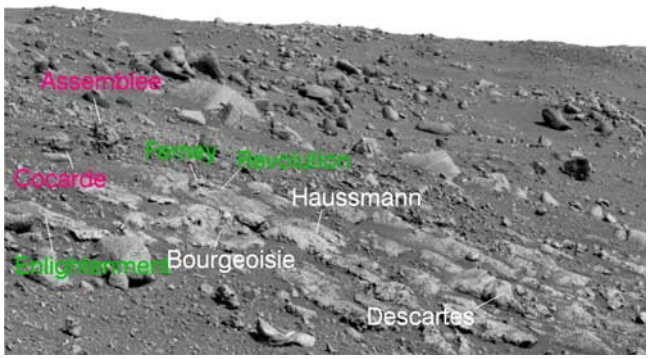

Figure 4. Portion of the sol 549 Pancam drive direction mosaic showing layered strata forming the Voltaire outcrops. The rocks strike from lower right to upper left (northeast to southwest) and dip into the hill (toward the southeast). Bourgeoisie, Haussmann, Descartes, and Assemblee are outcrops that were the focus of detailed in situ measurements by Spirit. Cocarde appears to have broken from Assemblee and moved slightly down hill. Both of these latter rocks have similar Mini-TES spectral emissivity signatures indicative of glassy materials. Enlightenment, Femey, and Revolution have emissivity signatures similar to one another and the rest of the Voltaire outcrops and also appear to be dominated spectrally by glassy materials. Pancam mosaic 2PP549ILFADCYL00P2352L777M2.

Table 4. Summary of Strikes and Dips Calculated for Voltaire Outcrops[a]

Sol and Frame Number	Strike (degrees)	Dip to Southeast (degrees)
565 2R176524254RSDADAEP1312L0MZ	N45E	35
565 2R176523021RSDA2P1301L0MZ	N29E	23
565 2R176524254RSDADAEP1312L0MZ	N48E	37
563 2F17634947RSLAD92P1121LOMZ	N75E	46

[a]Orientations for the bedding planes were derived from unit vector surface normal data computed from stereo observations using regions of interest defined by inspection to isolate bedding surfaces.

NE by a cover of soil and rocks (Figure 4). Specifically, detailed image analyses demonstrated the presence of a half dozen discrete layers striking ~60° clockwise from north and dipping to the southeast (Table 4). The Voltaire outcrops may be a discrete mélange block emplaced by impact or tectonic movements, or a tilted section of a more extensive exposure of bedrock.

[12] An extensive campaign was undertaken by Spirit in which a number of targets on outcrops (Descartes, Bourgeoisie, Haussmann, and Assemblee) were examined using both the remote sensing and in situ instruments (Table 3). The outcrops exhibit two basic morphologic patterns. Descartes, Bourgeoisie, and Haussmann are characterized by relatively smooth, tabular appearances with well-defined bedding and joint planes (Figure 5). A number of subrounded to rounded clasts ranging in size from a centimeter to a few centimeters are contained in these tabular outcrops, i.e., the deposits are conglomerates (Figure 5). The exposed clast surfaces have been shaped into ventifacts by wind erosion. The Chic clast on Bourgeoisie was the target of Microscopic Imager (MI), APXS, and MB observations, along with nearby matrix materials (Discourse and Gentil Matrice) (Tables 1, 3, 5, and 6). Additional matrix measurements were made on the Haussmann and Descartes outcrops. The second morphologic form is represented by the top-most portion of the Voltaire Outcrop (Assemblee; Tables 3–5 and Figure 6). This conglomeratic rock exhibits a nodular or crumbly appearance and when examined with the MI shows numerous relatively small and well rounded clasts (typically ~< 0.5 cm across) (Figure 6b) [*Clark et al.*, 2007]. Several other rocks with nodular textures similar to those for Assemblee can also be seen (e.g., Cocarde, Egalite; Figure 4), although as float rather than as outcrop. Assemblee was the only rock of this type for which MB, APXS, and MI data were acquired.

[13] Pancam multispectral observations were obtained for the Voltaire outcrops and surrounding rocks and soils and representative spectra are shown for Descartes and Assemblee surfaces in Figure 7. The absorption and scattering features for the spectral range covered by Pancam (0.4 to 1.0 μm) are controlled to first order by the abundance and textural characteristics of ferrous and ferric bearing minerals [e.g., *Burns*, 1993], including pyroxene, olivine, nanophase iron oxides, hematite, and goethite, all of which have been detected by Spirit's MB during its measurements on the Columbia Hills [*Morris et al.*, 2006, 2008]. The Pancam spectrum for the Descartes surface is brighter than the one for Assemblee and shows a steeper ferric absorption edge

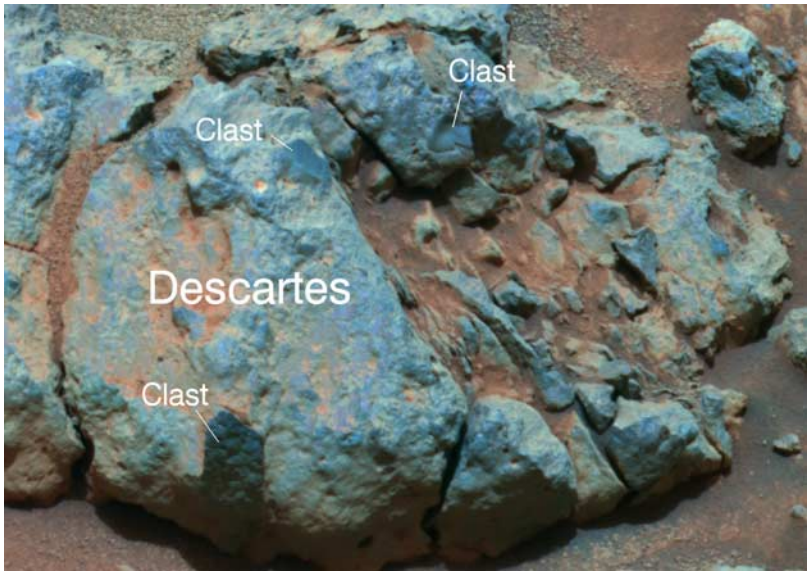

Figure 5. Pancam false color composite of the Descartes Outcrop oriented so that the bedding planes are parallel to the bottom of the image. Joints cut across the outcrop from lower right to upper left and can also be seen in the sol 549 approach mosaic (Figure 4). Locations of in situ observations are shown, including the Moncherie clast (bottom most labeled clast). Pancam frames 2P175278077ESFAD40P2558L2M1, 2P175278161ESFAD40P2558L5M1, and 2P175278228ESFAD40P2558L7M1 were used to generate the mosaic.

Table 5. MB-Based Percentage Iron Mineralogy for Key Targets From *Morris et al.* [2006, 2008]

Name	Olivine	Pyroxene	Ilmenite	Chromite	Nanophase Iron Oxide	Magnetite	Hematite	Goethite	Fe^{+3}/Fe_{total}
Descartes (A555RB0)	1	27	0	0	43	18	5	7	0.68
Chic (A559RB0)	26	25	18	0	23	7	2	0	0.31
Assemblee (A568RU0)	0	44	0	23	32	0	0	0	0.37
Cliffhanger (A609SU0) Cliffhanger_Hang2	13	41	0	0	30	7	9	0	0.45
El Dorado (A708SU0) Shadow	47	32	0	0	8	12	0	0	0.17
Halley (A836RU0) Halley_Offset	2	3	0	0	8	15	73	0	0.88
Esperanza (A1056RU0) Palma	4	45	0	0	4	45	1	0	0.40

between 0.4 to 0.8 μm. This is consistent with the MB and APXS observations that together show a threefold higher concentration of nanophase iron oxides and the presence of goethite (FeOOH) in Descartes as compared to Assemblee (Tables 5–6). The Descartes spectra show a band minimum between 0.9 to 1 μm, whereas the spectra for the Assemblee surface are relatively flat in this wavelength region. These patterns are consistent with the higher proportion of Fe-bearing minerals in Descartes (14.2% versus 6.4%, as FeO) based on APXS observations (summarized in Table 6) [*Ming et al.*, 2008] and the detection of iron-bearing pyroxene for both outcrops from MB data (Table 5). Although great care must be exercised in comparing Pancam spectra with MB and APXS data because of the different sampling depths in this case the patterns in the data imply that all three instruments are sampling the same materials.

[14] Mini-TES observations were acquired for a variety of rock targets during the extensive campaign of in situ observations on the Voltaire outcrops (Figures 8 and 9). The Mini-TES observations illustrate the synergistic use of the remote sensing elements of the Athena Payload (Table 1) in that the targeting for the observations took advantage of both Navcam and Pancam (including color) mosaics to cover the range of morphologic forms for the outcrops and float rocks within Spirit's field of view. Figure 8 shows the Mini-TES ''footprints'' projected onto a portion of a Navcam mosaic taken when Spirit was sitting on the Voltaire outcrops. On the basis of emissivity patterns the rocks can be divided into five distinct spectral classes (Figure 9). First, many of the boulders uphill from the Voltaire Outcrop are spectrally similar to the Wishstone float rock observed earlier in the mission and found in many places on Husband Hill, as determined from Pancam and Mini-TES observations (see Appendix A for Wishstone float rock location) [*Farrand et al.*, 2006; *Ruff et al.*, 2006]. The Wishstone-like emission spectra are dominated by stretching and bending vibrations of plagioclase feldspar of an intermediate composition, as shown in Figure 9. A second and relatively rare class consists of boulders with spectra similar to the basaltic rock, Backstay (encountered earlier on Husband Hill, see Appendix A for location), based on olivine and pyroxene stretching and bending vibrational modes (Figure 9). A third and also relatively rare class of float rock is spectrally similar to the olivine-bearing basalt rocks that dominate the plains (i.e., similar to Adirondack and represented by Liberte; Figures 8 and 9). The abundance of Wishstone materials and their altered equivalents, Watchtower materials [e.g., *Ming et al.*, 2008], on Husband Hill implies that the top of the antiformal stratigraphic section is dominated by these materials. Mapping by us shows that the Voltaire Outcrop is stratigraphically below Wishstone materials and includes the nearby Independence Outcrop (Appendix A).

[15] Emissivity spectra for the Voltaire outcrops show a fourth and fifth pair of spectral classes that are distinctly different from those discussed in the previous paragraph. In particular, the Descartes class is characterized by broad, relatively featureless absorption in the low-wave-number region (<600 cm^{-1}) and dominates the spectral appearance for Descartes, Bourgeoisie, and Haussmann Outcrop observations. The spectra are consistent with the presence of an amorphous silicate phase and also share similarities with the typical ''dust'' spectra identified in many places using Mini-TES data. Spectra for Assemblee form the fifth class and show a distinct emissivity minima at ~1050 cm^{-1} and ~460 cm^{-1} (Figure 9) and are similar to spectra for the outcrop, Clovis, on West Spur (see Appendix A for Clovis location and *Ruff et al.* [2006] for further spectral details). The broad nature of these two emissivity minima is similar to the spectra of glassy or amorphous silicate phases [e.g., *Parke*, 1974]. There are also spectra for float rocks near the Voltaire outcrops that match a mix of materials and are thought to represent Voltaire Outcrop materials that have been weathered and left exposed as boulders (Figure 8).

[16] The Mini-TES footprint is too large to isolate Voltaire Outcrop clast material. However, MB and APXS observations provide compelling evidence that the clasts are dominated by Wishstone-type materials (Tables 5 and 6).

Table 6. APXS Compositional Data From *Ming et al.* [2006, 2008]

	Oxides (wt %)													Elements (mg/kg)			
	SiO_2	TiO_2	Al_2O_3	FeO	MnO	MgO	CaO	Na_2O	K_2O	P_2O_5	Cr_2O_3	Cl	SO_3	Ni	Zn	Br	Ge
A552_OU_Descartes_Discourse	45.32	0.97	9.93	14.29	0.24	9.35	5.56	3.14	0.61	1.38	0.17	1.30	7.64	436	209	155	15
A566_OU_Assemblee_Gruyere	51.01	0.79	17.39	6.43	0.15	8.21	3.77	1.70	0.93	1.60	2.86	0.92	4.03	1248	244	65	22
A611_SU_Cliffhanger_Hang Two	47.73	1.20	12.34	10.77	0.22	7.24	7.13	3.60	0.51	2.10	0.13	0.78	6.16	168	155	104	4
A709_SU_El Dorado_Shadow	46.91	0.62	10.74	15.96	0.31	11.31	6.10	3.01	0.31	0.81	0.32	0.38	3.06	997	114	22	0
A833_SU_Enderbyland_Halley Center	45.30	0.90	8.73	17.97	0.24	9.31	5.30	2.71	0.60	0.90	0.19	0.86	6.67	777	2270	32	17
A1055_RU_Esperanza_Palma	47.9	1.05	8.40	20.2	0.38	8.45	5.57	3.40	0.52	0.91	0.20	0.47	2.36	395	368	181	19

Figure 6a. Pancam false color view of the Assemblee Outcrop showing the target Gruyere that was the focus of in situ measurements. Note the friable nature of this outcrop. The rock strikes from lower right to upper left (SW to NE) and dips into the hill (toward the SE). The Pancam frames used were 2P175540927ESFAD56P2566L2M1, 2P175541009ESFAD56P2566L5M1, and 2P175541077ESFAD56P2566L7M1.

This conclusion is strengthened by use of correspondence analysis applied to APXS elemental compositional data for rocks from the hills (Figure 10). Correspondence analysis is a powerful technique for exploring structure and relationships among samples and variables in a multidimensional data set. It is a form of principal component analysis in which normalization of the data matrix allows plotting of factor loadings for both samples and variables using the same scales [e.g., *Arvidson et al.*, 2006a, 2006b]. In particular, analyses for the matrix material on Descartes, Bourgeoisie, and Haussmann show that these targets plot close to compositional origin (i.e., the average) of rocks analyzed in the Hills. The Chic clast (in the Bourgeoisie Outcrop) has a composition displaced toward the Wishstone sample location when projected onto the first two factor vectors (Figure 10). It also shows that Assemblee is enriched in Cr_2O_3, SiO_2, K_2O, and Al_2O_3 and depleted in FeO relative to the matrix material in the other Voltaire outcrops. In fact, removal of Cr_2O_3 and recomputing the factor loadings show that Assemblee and Independence have compositional similarities, a pattern also noted by *Clark et al.* [2007]. Assemblee is also enriched in Ni and Ge relative to the other matrix materials in the Voltaire outcrops (Table 6).

[17] The amorphous material in the Voltaire outcrops detected by Mini-TES cannot be iron-bearing glass since this material would have also been detected by the MB instrument for Descartes, Bourgeoisie, and Haussmann, and Assemblee (and Clovis) and was not (Table 5) [*Morris et al.*, 2006, 2008]. Rather the iron-bearing minerals in the outcrops (with the exception of clasts) are dominated by nanophase iron oxides and pyroxene. The Descartes matrix also has magnetite, hematite, and goethite present whereas Assemblee has chromite as a third phase.

[18] The ensemble of data collected for the Voltaire experiments allows development of a working hypothesis for the formation and alteration of these outcrops. The conglomeratic nature of the outcrops, combined with the evidence for an amorphous or glassy component, argues for emplacement as an impact melt that incorporated local Wishstone materials, although emplacement as an energetic volcanic flow or pipe cannot be ruled out. Postemplacement alteration in an aqueous environment is indicated by the detection of goethite (FeOOH) in the Descartes Outcrop (Table 5). The presence of nanophase iron oxides, hematite, and goethite in Descartes and nanophase iron oxides in Bourgeoisie, and Haussmann outcrops, combined with the fact that none of the glassy or amorphous phases detected by Mini-TES are ferrous- or ferric-bearing, provide additional clues for the alteration history of these materials. We envision a process of in situ alteration of the glassy phase in these rocks, releasing iron to form iron oxides and goethite, not unlike a terrestrial process in which allophane and iron oxides and oxyhydroxides are generated in soils weathered from basaltic rocks [*Parfitt and Furkert*, 1980] and glassy basaltic tephra [e.g., *Morris et al.*, 2000]. Chromite in Assemblee (Table 5) may have remained immobile during this process. The Si and Ge enhancements and low FeO in Assemblee relative to the rest of the Voltaire measurements (Table 6) are consistent with the trends seen in Hawaiian soils formed from relatively intense aqueous weathering of basaltic rocks, i.e., SiO_2 and Al_2O_3 and Ge concentrate in the soils while FeO is removed by aqueous processes [*Morris et al.*, 2000; *Kurtz et al.*, 2002; *Ming et al.*, 2008]. Finally, we note that *Schmidt et al.* [2008] concluded from analyses of Mini-TES spectra that glassy or amorphous components are indeed widespread in the Columbia Hills sites visited by Spirit, although no iron bearing glassy phases have been detected by MB [*Morris et al.*, 2008].

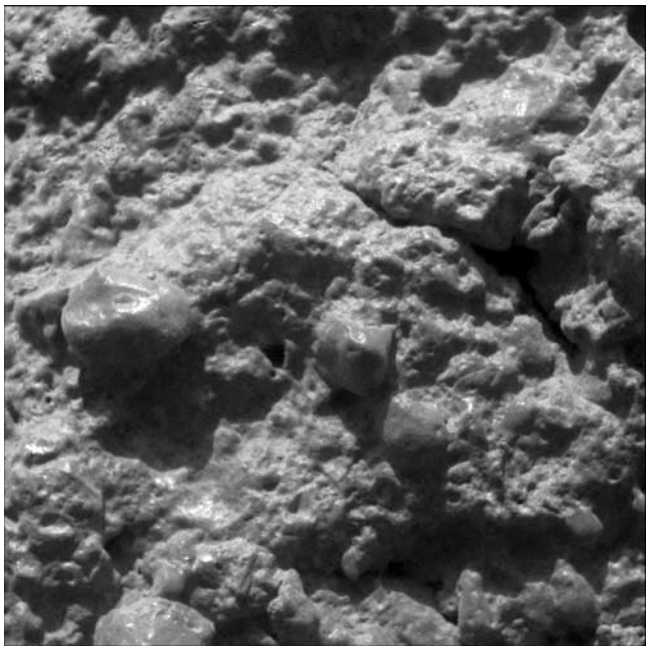

Figure 6b. MI frame of Gruyere showing the presence of rounded, embedded clasts. Frame covers ~3 cm across. Frame number 2M176609837EFFADAEP2936M2F1.

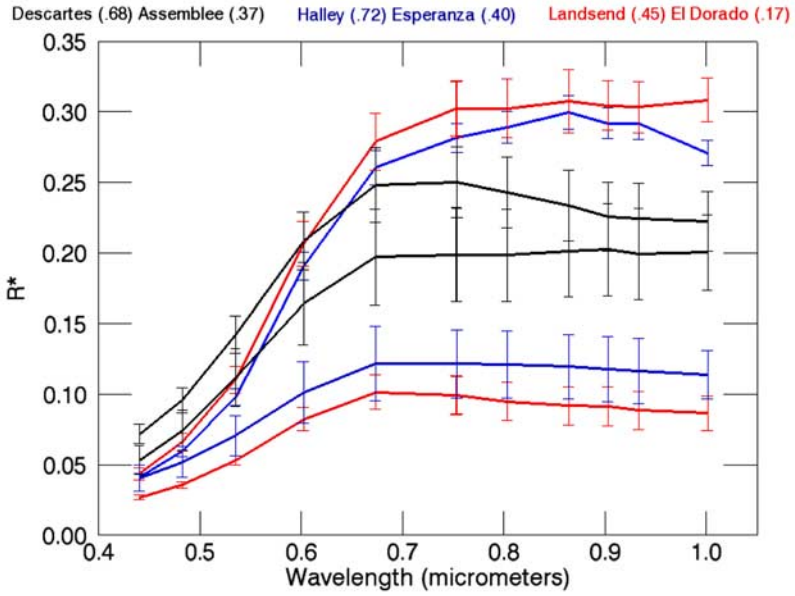

Figure 7. Pancam spectra for a series of features discussed in this paper. The legend at the top of the figure denotes the feature names. Numbers in parentheses represent the Fe^{+3}/Fe_{total} ratios derived from MB measurements for targets on the relevant features. The brighter spectra have higher ratios. Error bars represent 1 standard deviation about the mean values for the group of pixels used to generate the spectra. All the spectra show a strong ferric oxide absorption edge typical for Mars. Longer-wavelength features are also diagnostic of mineralogy and are discussed in detail in the text. *R** is equivalent to Lambert albedo. The Pancam frames used are as follows: Descartes (p2558, Sol 551), 2P175278077IOFAD40P2558L2C1; Assemblee (p2541, Sol 572), 2P177142010IOFADAEP2541L2C1; El Dorado (p2536, Sol 711), 2P189482458IOFAL02P2536L2C1; Cliffhanger (p2587, Sol 611), 2P180607674IOFAEM9P2587L2C1; Halley (p2286, Sol 925), 2P208478741IOFAS00P2286L2C1; Esperanza (p2599, Sol 1070), 2P221351648IOFASCGP2599L2C2.

Thus the process described above may have been a common and widespread phenomenon that altered glassy deposits.

4. Inner Basin: Volcanic Rocks and Associated Deposits

[19] Spirit entered the Inner Basin of the Columbia Hills after descending Husband Hill and Haskin Ridge, spending >800 sols exploring the landforms and deposits in and around the ~80 m wide ovoidal plateau termed Home Plate (Figures 2a–2d and Table 2). Rock exposures on the flanks of Home Plate are dominated by volcanic tuff deposits that show evidence for energetic explosive emplacement, including cut and fill structures, cross bedding, and a "bomb sag" produced when a block was ejected into the atmosphere and impacted into deformable tuff deposits [*Squyres et al.*, 2007; *Lewis et al.*, 2008]. Interaction of subsurface magma with groundwater is the likely cause of the explosive volcanism.

[20] Mitcheltree Ridge and Low Ridge (Figures 2 and 11), located to the east and southeast of Home Plate, respectively, are capped by vesicular basalt boulder fields and wind-blown soils (Figure 11). The rock, Esperanza, examined by Spirit after leaving the Low Ridge Winter Campaign site, is an example of one of these boulders (Table 2 and Figures 11–13). Examination of the MI coverage of Esperanza shows that the vesicles have been finely shaped by wind, forming a series of sharp edges typical of wind-sculpted vesicular basalt outcrops and boulders on Earth (Figure 12b). In fact the MI data show sand, the likely abrasive agent, sitting in one of the vesicles. MB observations of Esperanza indicate subequal amounts of iron within pyroxene and magnetite, with a minor component in nanophase iron oxides (Table 5). Pancam spectra for Esperanza are consistent with the presence and relative abundances of these minerals in that the spectra are dark (consistent with relatively high magnetite concentration) and show a slight downturn at longer wavelengths consistent with the presence of pyroxene (Figure 7). Mini-TES spectra are dominated by the presence of pyroxene bending and stretching mode vibrations [see also *Schmidt et al.*, 2008] and are similar to the spectra for Bounce Rock, a pyroxenite examined in detail by Opportunity in Meridiani Planum (Figure 13).

[21] Thinly bedded, platy outcrops of granular materials composed of sand-sized grains are found near the bottom of both Low Ridge and Mitcheltree Ridge and the outcrop, Troll, located between the two Ridges (Figures 11 and 2d). Detailed mapping using Navcam panoramic images acquired from the Low Ridge winter campaign site, during traverses to and from Tyrone, and while Spirit was located in the Eastern Valley between Home Plate and the Ridges (Figure 2d), shows that these platy deposits are found on both western and eastern sides of the ridges and are dominated by dips into the Ridges [*Lewis et al.*, 2007]. The deposits on the northern side of Low Ridge define dips

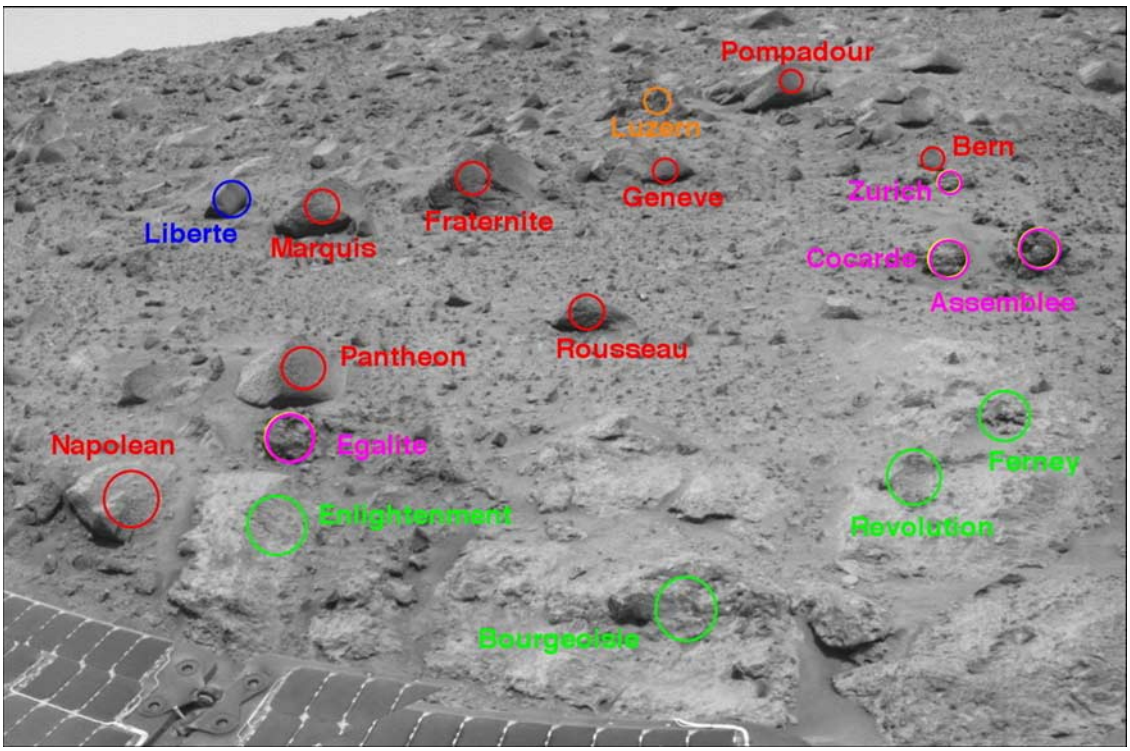

Figure 8. A subset of the Navcam mosaic acquired on sol 551 looking to the northeast, with color-coded footprint locations for acquisition of Mini-TES spectra overlain. Green colors correspond to the Descartes class spectrum shown in Figure 9. Magenta corresponds to the Assemblee spectral class. Red corresponds to a Wishstone-like, orange corresponds to a spectral mix of Assemble and Wishstone, and blue corresponds to an Adirondack-like spectrum. The Backstay spectral class is not shown on this mosaic. Note the dominance of Wishstone-like materials toward the uphill section of the image. Navcam mosaic 2NN551EFFADCYL56P0660L00M1.

that wrap around and form the northern nose of a synclinal structure. Thinly bedded, platy outcrops are also evident on the eastern flank of Home Plate and dip to the west. Thus the outcrops on the Eastern Valley floor between Home Plate and the Ridges are exposed as the core of an antiformal structure.

[22] The dominant materials exposed in the Eastern Valley, in addition to wind-blown soils, are platy, buff colored outcrops. Halley is one of these outcrops and was examined in detail while Spirit was parked for the winter at Low Ridge (Table 2 and Figure 11). MI images show that this platy outcrop is fine grained. MB data show that Halley's iron-bearing minerals are dominated by hematite and that this outcrop has a very high Fe^{+3}/Fe_{total} ratio (Table 5). Pancam spectra extracted for Halley and surrounding platy outcrops show a high overall albedo, pronounced ferric slope between 0.4 and 0.8 μm, an increasing reflectance with increasing wavelength out to $\sim$0.9 μm, a minor inflection at $\sim$0.9 μm, and a relatively sharp negative spectral slope between $\sim$0.9 and 1.0 μm (Figure 7). The sharp down turn for light-toned disturbed soils in the Eastern Valley observed by Pancam has been interpreted by *Rice et al.* [2008] as an O-H stretch overtone or a water combination band resulting from the presence of hydrated or hydroxlated mineral phases. On the basis of extensive APXS observations, Halley may contain calcium sulfate minerals, e.g., gypsum or anhydrite [*Yen et al.*, 2008; *Ming et al.*, 2008]. The ensemble of evidence for Halley implies that hermatite and hydrated or hydroxlated sulfate-bearing phases are present.

[23] The thinly bedded, platy outcrop, Graham Land (King George Island target), is located stratigraphically above the Halley deposits and was examined by Spirit as it left the winter campaign site (Figure 11). MI data show that this outcrop is dominated by round, very coarse sand-sized grains, and MB data show that hematite dominates the iron-bearing mineralogy (Table 5 and Figure 14). Additional and similar deposits (Montalva and Riquelme) were examined by Spirit when it parked at the adjacent Troll Outcrop and the ensemble of data again show that these deposits are platy, granular, and that iron-bearing materials are dominantly in hematite. In fact, correspondence analysis applied to MB data for all rocks found within the Inner Basin shows a progressive enrichment in hematite relative to other iron bearing minerals for the platy outcrops found on the Ridges and within the Eastern Valley (Figure 15).

[24] As noted, the platy outcrops exposed in the Eastern Valley between Home Plate and the Ridges are largely covered by a thin veneer of wind-blown soil. In some locations the platy outcrops are covered not by soils but by clasts that exhibit a nodular appearance (Figure 16). These nodular materials, where examined by Spirit's Mini-TES and APXS instruments, were found to be outcrops of silica-rich materials or debris fields of the same type of

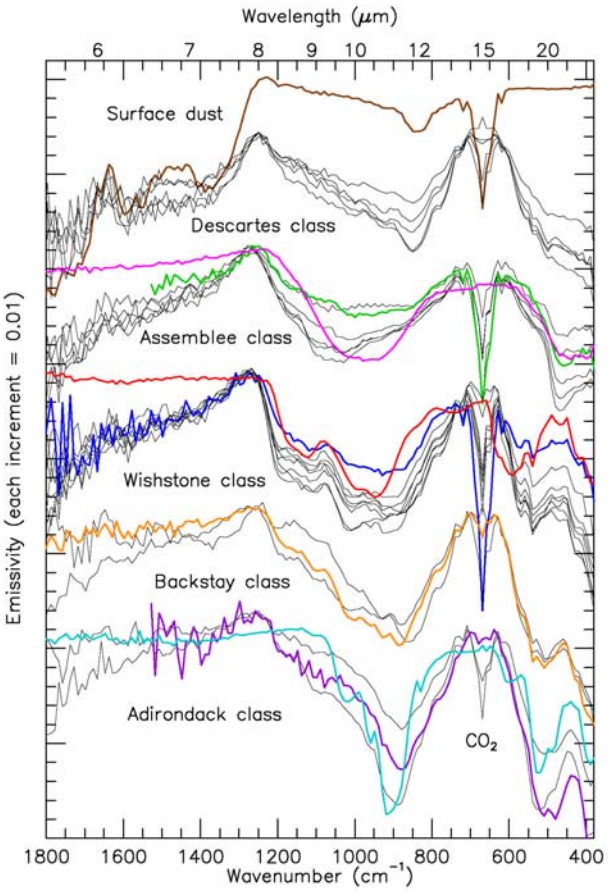

Figure 9. Mini-TES spectra (in black) from the Voltaire region compared with laboratory and other Mini-TES spectra in colors. Descartes spectra have a significant dust component as evident from the scaled Gusev dust spectrum (brown) and the relatively featureless low-wave-number region (<600 cm^{-1}) is consistent with a mixture containing an amorphous silicate phase like basaltic glass (magenta; scaled laboratory). Assemblee spectra are dominated by an amorphous silicate phase like basaltic glass (magenta) and among all Mini-TES spectra from Gusev crater, most resemble Clovis class rocks (green). Wishstone spectra are dominated by intermediate plagioclase (labradorite shown in red; scaled) and clearly match the type example (blue, an average of four spectra) from earlier in the mission. Backstay and Adirondack spectra (orange and purple, respectively) compare favorably to the subset of float rock spectra shown. Adirondack spectra are dominated by olivine, as shown by the scaled laboratory-based spectrum (cyan) that is an average of 60% forsteritic olivine and 35% forsteritic olivine compositions. Adirondack was examined early in the mission on the plains [*Arvidson et al.* 2006a].

materials crushed by the vehicle's inoperative right-front wheel [*Squyres et al.*, 2008, Figure 16]. Mini-TES spectra indicate the presence, in particular, of opaline silica, and APXS data for the Gertrude Weise disturbed soils show that the material is almost pure silica (~90%) with the remaining component consisting largely of TiO_2 [*Squyres et al.*, 2008, Figure 17]. These materials are inferred to have been deposited by aqueous fluids under acid-sulfate low pH conditions by either dissolution and reprecipitation in-place or transport in solution to the depositional location [*Squyres et al.*, 2008]. Additional support for the presence of acid-sulfate fluids is the presence of hydrated sulfate deposits in soils disturbed by Spirit's wheels in the Inner Basin to the north of Home Plate (Arad feature) and to the east of Mitcheltree Ridge (Tyrone feature; Figures 2 and 11). Emissivity spectra indicate the presence of hydrated materials based on the presence of a ~6 μm feature attributed to the fundamental bending mode of water, MB data show the presence of a ferric-sulfate phase, and APXS data show that SO_3 increases with increasing SiO_2 concentrations (Figure 17) [*Morris et al.*, 2008; *Yen et al.*, 2008; *Wang et al.*, 2008].

[25] The results from the data collected by Spirit in and around Home Plate allow development of a model that focuses on the Inner Basin volcanic history and the role of aqueous fluids in emplacement and modification of the deposits. As noted, Home Plate has been interpreted to be a partially eroded volcaniclastic construct [*Squyres et al.*, 2007]. Acid sulfate aqueous activity (vapor and/or fluids) occurred as the volcaniclastic deposits formed, interleaving silica-rich and sulfate-rich deposits, and altering some of the ash materials to hematite and other phases. For most of its history wind erosion has probably dominated changes in the Inner Basin, differentially stripping the materials to produce the landforms, outcrops, and soil exposures explored by Spirit.

[26] The Kau Desert, Kilauea, Hawaii is offered as an Earth analog for the generation of volcaniclastic materials, lava flows, and formation of silica-rich and sulfate-rich deposits in the Inner Basin (Figure 18). In the Kau Desert, basaltic ash deposits are found interleaved with basaltic lava flows. Some of the ash deposits formed as rounded, well sorted, and oxidized accretionary lapilli produced when wet ash clouds caused nucleation of fine airborne ash into spherical sand grains. This is a plausible explanation for the finely layered, platy, granular deposits evident in the King George Island Outcrop and elsewhere in the Inner Basin ridges (Figure 14). Opaline silica encrustations are common in the Kau Desert and form in the vicinity of steam vents by dissolution of rock and in-place precipitation of opaline silica, and as case-hardened, but friable coatings on ash deposits created as silica-rich solutions evaporated when they reached the surface [*Malin et al.*, 1983; *Schiffman et al.*, 2006; K. Seelos et al., Silica in a Mars Analog Environment: Ka'u Desert, Kilauea Volcano, Hawaii, manuscript in preparation, 2008]. Further, in some locations acid-sulfate rich solutions have thoroughly altered basaltic materials and left behind silica-rich residues. Sulfate deposits (e.g., primarily gypsum, minor amount of jarosite) also form near steam vents, although the minerals are retained primarily where protected (beneath overhangs or within internal cavities within lava flows) from rainfall and dissolution (Seelos et al., manuscript in preparation, 2008).

5. Coordinated Analyses of Orbital and Spirit-Based Data Sets

[27] The previous sections of this paper have highlighted the extensive exploration and measurement campaigns conducted by Spirit in the Columbia Hills and focused on

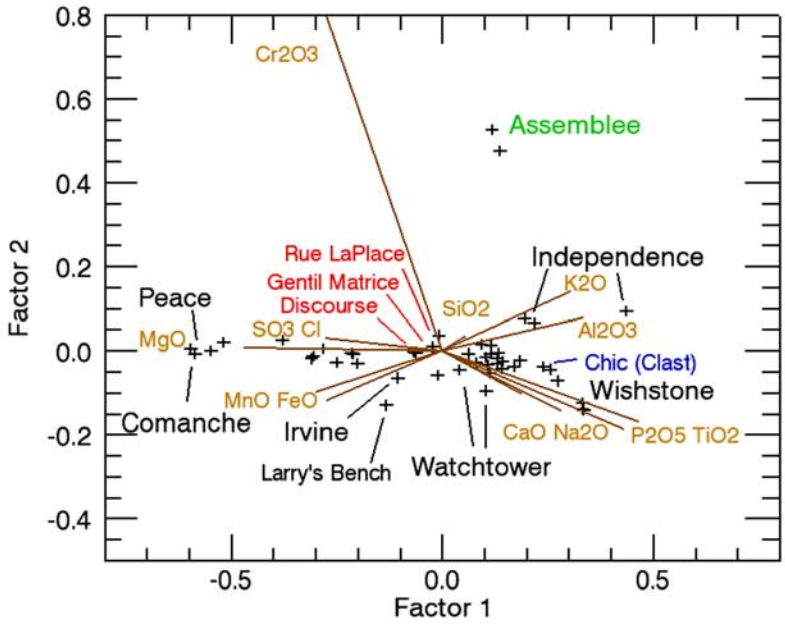

Figure 10. APXS-based factor 1 versus 2 plot from a correspondence analysis run for rocks examined on Husband Hill. This plane captures 83% of the variance of the APXS data set and shows how rock analyses relate to one another and which elements provide "finger prints" or distinguishing characteristics for the samples. For example, Independence is enriched in SiO_2, K_2O, and Al_2O_3, whereas Wishstone is enriched in CaO, Na_2O, P_2O_5, and TiO_2 relative to the average composition for rocks examined on Husband Hill. The rock analyses shown in red are for matrix materials (Discourse on the Descartes Outcrop, Gentile Matrice on the Bourgeoisie Outcrop, and Rue LaPlace on the Haussmann Outcrop), whereas the blue color corresponds to Chic, a clast in the Bourgeoisie Outcrop. Note that the matrix materials plot close to the composition average for the rocks, whereas Chic is displaced toward Wishstone. Assemblee is highly enriched in Cr_2O_3 and is enriched in SiO_2, K_2O, and Al_2O_3 and plots as a very chemically distinct rock relative to other rocks examined on Husband Hill. APXS data from *Ming et al.* [2006] and *Ming et al.* [2008].

two examples that show that water was involved in alteration of crustal materials: the Voltaire outcrops and the emplacement and modification of volcanic materials in the Inner Basin. The discovery of evidence for extensive aqueous alteration is in contrast to what was found by Spirit during its exploration of the volcanic plains that surround and embay the Hills. Specifically the plains are dominated by olivine-bearing basaltic float rocks and wind-blown soils that are weakly altered relative to the rocks in the Hills [*Arvidson et al.*, 2006a; *Haskin et al.*, 2005; *McSween et al.*, 2008; *Morris et al.*, 2008; *Ming et al.*, 2008]. The question is: Can the evidence for aqueous alteration in the Columbia Hills also be detected from orbit?

[28] Analysis of Mars Global Surveyor Thermal Emission Spectrometer (TES) data [e.g., *Martinez-Alonso et al.*, 2005] and Mars Express OMEGA hyperspectral imager data (0.4 to 5 μm) [*Lichtenberg et al.*, 2007] for the Gusev plains are also consistent with the presence of slightly oxidized basalt sands mixed with and covered to varying extent with dust. Neither orbital instrument can resolve landforms within the Columbia Hills since the pixel size for TES is $\sim$3 km and at best $\sim$350 m for OMEGA. Thus data from TES and OMEGA cannot be used to test the hypothesis that Spirit's observations in the Columbia Hills of glassy or amorphous deposits, goethite, hematite, opaline silica, and hydrated sulfates can also be detected from orbital observations. On the other hand, the CRISM hyperspectral imager on MRO acquires Full Resolution targeted (FRT) mode data from 0.4 to 4.0 μm (545 bands, 18 m/pixel, $\sim$10 km frame width) and is able to resolve many of the features within the Columbia Hills, including Husband Hill, El Dorado, and the Inner basin (Figure 1). In this section of the paper, reduction and analysis of CRISM observations are detailed and conclusions drawn about what controls the spectral signatures of the Columbia Hills at the spatial scale sampled by this instrument.

[29] Several CRISM Full Resolution targeted (FRT) mode observations were acquired of the Columbia Hills and surrounding areas while Spirit obtained near simultaneous atmospheric optical depth measurements using the Pancam cameras to image the sun at 0.4 and 0.8 μm and Mini-TES to obtain temperature profiles of the lower atmosphere. These observations and dust and ice aerosol radiative properties based on historical trends from TES data were used with the DISORT radiative transfer code [*Stamnes et al.*, 1988] to model CRISM's spectral radiances. Atmospheric carbon dioxide, water vapor, carbon monoxide, and associated Rayleigh scattering and discrete gas absorption bands for CO_2, H_2O, and CO were included in the computations, along with aerosol scattering and absorption. Procedures were implemented to retrieve surface

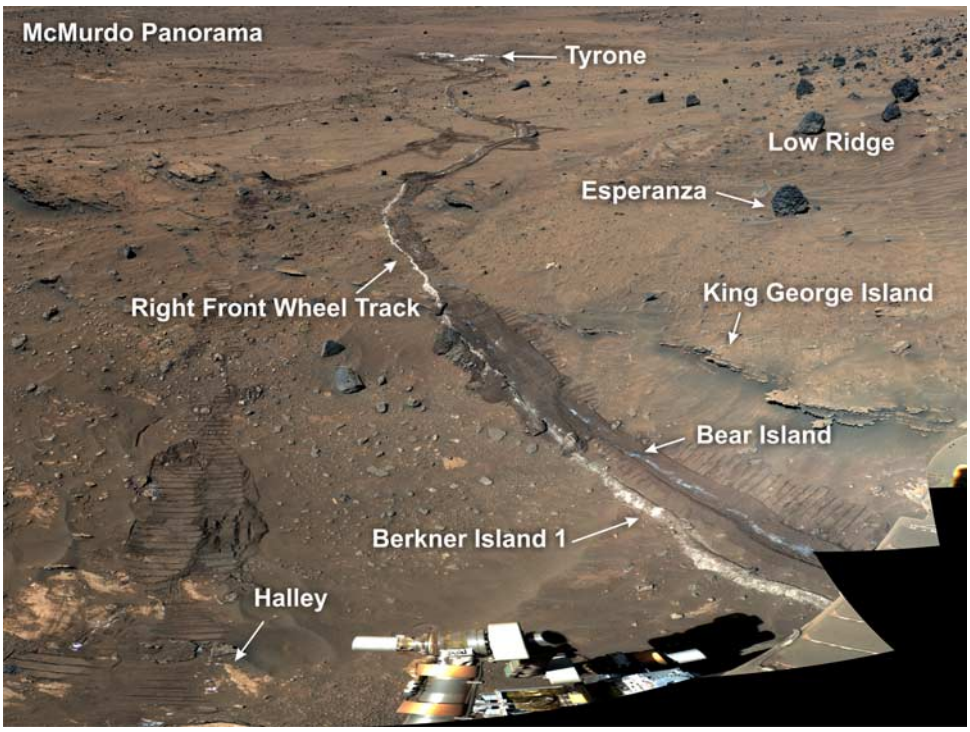

Figure 11. Portion of McMurdo Pancam panorama acquired from the Low Ridge winter campaign site looking to the northeast. The light-toned Tyrone disturbed soils can be seen in the distance, along with tracks leading to and from Tyrone, and the light-toned soils spilled from the right front wheel cowling during Spirit's backward drive from Tyrone to the winter site. Berkner Island is the light-toned soil target examined in detail by Spirit with its in situ instruments. King George Island is the platy outcrop target that dips into Low Ridge and that was examined by Spirit, along with the vesicular basalt boulder Esperanza immediately after leaving the campaign site in the spring. Halley and Bear Island were also examined in detail as part of the winter campaign. The Troll Outcrop, located in the upper left portion of the figure, was another location for detailed measurements after leaving the campaign site. Platy outcrops typified by King George Island wrap around Low Ridge and form a synformal structure. Color image using the 0.43 for blue, 0.53 for green, and 0.60 μm for red.

Lambert albedos using DISORT-based simulations and regressions for each wavelength band between modeled CRISM radiances and a suite of input gray surface albedos, following the methodology outlined by *Arvidson et al.* [2006b] for modeling OMEGA data over the Opportunity site. The retrieved surface spectra were examined for residuals associated with changes in band pass characteristics relative to prelaunch calibrations and incomplete removal of atmospheric carbon dioxide and water vapor. Runs with updated band pass values and atmospheric conditions relative to historical trends and rover-based observations allowed convergence on the proper atmospheric model within several iterations.

[30] We concentrate on CRISM FRT00003192_07 acquired over the Columbia Hills and surrounding plains while Spirit was located at the Low Ridge winter campaign site (Figure 1). Detailed analysis of the CRISM spectra for the plains does not show any spectral evidence of the phyllosilicates, hydrated sulfates, or opaline silica deposits found elsewhere on the planet using OMEGA and CRISM observations [e.g., *Gendrin et al.*, 2005; *Arvidson et al.*, 2005; *Poulet et al.*, 2005; *Mustard et al.*, 2008; *Milliken et al.*, 2008]. A detailed search was also conducted using the CRISM data over the Columbia Hills for spectral signatures from (1) Voltaire and Voltaire-like materials (e.g., water combination bands at 1.4 and 1.9 μm, metal-OH features from allophane-like materials between 2 and 2.5 μm); (2) opaline silica signatures expected from deposits such as the disturbed soils in Gertrude Weise (e.g., the broad 2.2 μm Si-OH absorption and the 1.9 μm H_2O combination band detected using Airborne Visible and Infrared Imaging Spectrometer (AVIRIS) data in the Kau Desert, Hawaii (Seelos et al., manuscript in preparation, 2008) and from CRISM data for selected plains around Valles Marineris [*Milliken et al.*, 2008]); and (3) multiple H_2O combination bands associated with hydrated sulfates (e.g., water combination bands between 1 and 2.5 μm). None of these signatures was detected, even when precisely locating Spirit's experiment sites and examining single pixel spectra for these regions. Instead, the Columbia Hills CRISM spectra are dominated by the ferric-rich dust (spectrally dominated by nanophase iron oxides), olivine, and pyroxene, as will be detailed in the next several paragraphs. The data do show the ubiquitous $\sim$3 μm band found across Mars and associated with adsorbed or absorbed water molecules. The lack of vibrational bands associated with hydrated or hydroxlated minerals (i.e., items 1–3 above) is not surprising considering that the length scale for the Voltaire Outcrop is only $\sim$5 m

Figure 12a. Portion of the McMurdo Pancam panorama shown in Figure 11 enlarged to show details of Esperanza, interpreted to be a vesicular basalt boulder. The IDD target Palma is located on the left side of Esperanza out of site of the view shown. A second boulder is evident to the upper left of Esperanza and is interpreted to be a fine-grained rock shaped by wind into a ventifact. Esperanza is approximately 0.20 m across.

by 2.5 m and the rocks are surrounded and partially covered by wind-blown soil (Figure 4). In addition, the opaline silica and sulfate soils examined by Spirit were discovered only after the vehicle exposed them during drives (Figures 11 and 16), while the silica-rich nodular outcrops are small and heavily contaminated by wind-blown soil. The deposits may be widespread, but they are hidden from CRISM by a cover of wind-blown soil. Finally, no signatures expected from phyllosilicate minerals were detected for any spectra extracted from the Columbia Hills.

[31] Detailed examination of the CRISM data for the Columbia Hills regions traversed by Spirit shows that the spectral end-members are represented by the top of Husband Hill and the upper slopes of Tennessee Valley for the brightest area and the El Dorado ripple field for the darkest area (Figures 1, 2, and 19). On the basis of imaging data acquired while Spirit was at the summit of Husband Hill, combined with examination of the HiRISE data covering the summit and Tennessee Valley, it is clear that the upper portion of Tennessee Valley and the northern portion of the summit are covered by light-toned ripples that have migrated from the NW, i.e., up the valley (Figures 2a and 2b) [*Sullivan et al.*, 2008]. Spirit examined one of these ripples (Cliffhanger) during its summit experiments (Table 2 and Figures 2b and 20). The experiments included measurements of undisturbed and scuffed soils in the ripple. MB observations of the undisturbed (Hang2) and scuffed (Lands End) ripple soils indicate in order of decreasing abundance: pyroxene, nanophase iron oxides, olivine, hematite, and magnetite (Figure 20 and Table 5). Spirit also conducted similar experiments on the eastern edge of the El Dorado

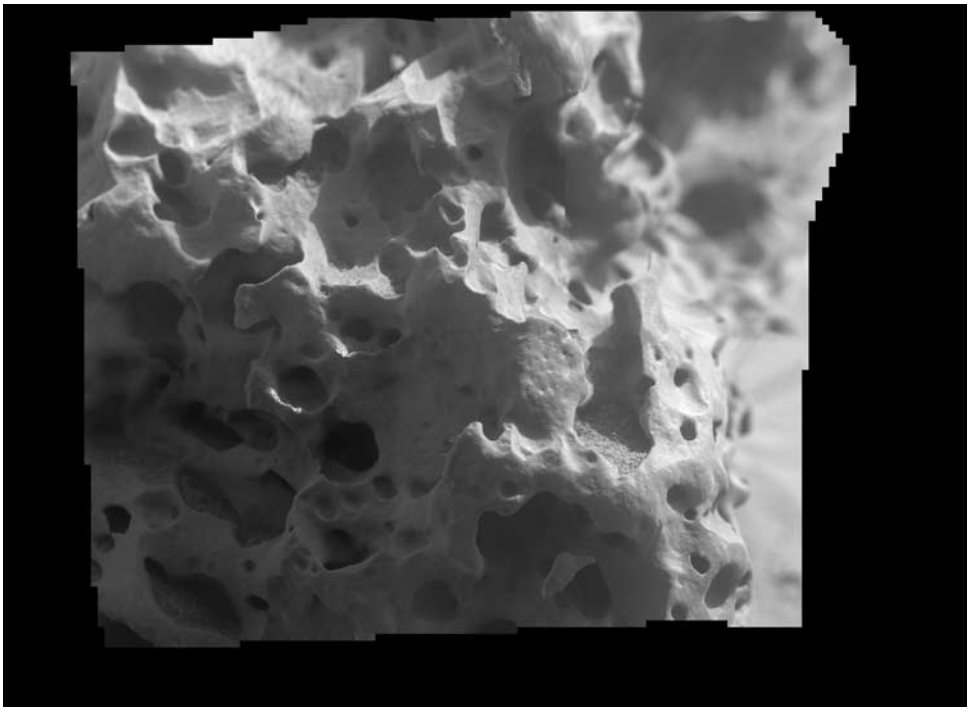

Figure 12b. MI mosaic of Esperanza illustrating the extent to which wind-blown sand and dust has shaped the surface into a set of sharp curvilinear ridges. Note the sand sitting on the bottom of one of the vesicles. Frame covers ~6 cm across. Mosaic 2MMA53IOFASORTAFP2936M222F1 with a filtering and contrast enhancement applied to minimize loss of detail from shadows.

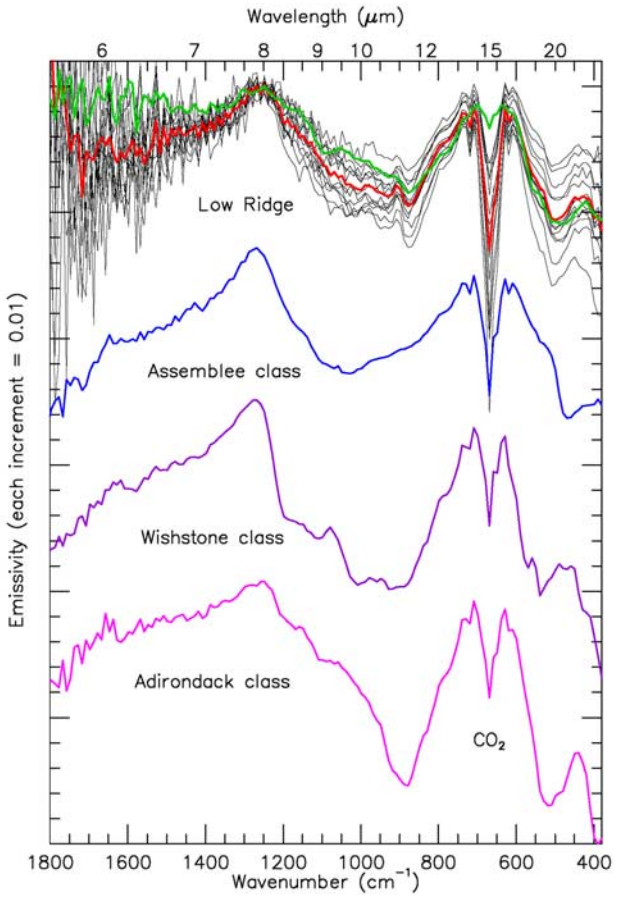

Figure 13. Mini-TES spectra for Esperanza and 12 other vesicular rocks from Low Ridge are shown in black (red is the average) and overlain with the pyroxene-rich Bounce rock spectrum (in green; this rock is a pyroxenite from Meridiani Planum and was observed by Opportunity) to demonstrate a spectral dominance by pyroxene. Pyroxene-rich rocks represent another spectral class of rock observed by Mini-TES that includes those dominated by glass or amorphous phases as represented by the average Assemblee spectrum (blue), the plagioclase-dominated Wishstone spectrum (purple), and the olivine-dominated spectrum represented by Adirondack basalt (magenta).

ripple field (Table 2 and Figures 2c and 21), with MB measurements from the undisturbed surface (Shadow) indicating in order of decreasing abundance: olivine, pyroxene, magnetite, and nanophase iron oxides (Table 5). Mini-TES spectra extracted for these surfaces indicate a dominance of olivine for the El Dorado area based on the bending vibrational modes evident between ~650 to 400 cm^{-1} and a dust dominance for the Cliffhanger ripple surfaces based on the overall spectral shape (Figure 22). Pancam spectra retrieved for Cliffhanger and El Dorado undisturbed surfaces are similar in overall shape to the CRISM spectra and consistent with a dominance of nanophase iron oxides in the visible wavelengths, olivine and pyroxene for longer wavelengths for the El Dorado spectra, and nanophase iron oxides and pyroxene for the light-toned ripples that dominate the western summit of Husband Hill and the upper Tennessee Valley (Figures 7 and 19). The El Dorado spectra also indicate a thin coating of dust that becomes translucent or more forward scattering with increasing wavelength, thus allowing the darker mafic sand to spectrally dominate. This phenomenon produces a negative slope as documented analyses of OMEGA data by *Lichtenberg et al.* [2007] for the Gusev plains and shown in the laboratory by *Fischer and Pieters* [1993] and *Johnson and Grundy* [2001].

[32] *Sullivan et al.* [2008] show that El Dorado is a ripple field that accumulates a thin coating of dust that locally is removed by dust devils. The light-toned ripples on the top of Husband Hill, on the other hand, are more coarse grained and interpreted to be active only during rare high velocity wind events capable of moving the coarse particles and otherwise develop a uniform dust cover [*Sullivan et al.*, 2008]. An optically thick dust cover is certainly consistent with the observation that the Pancam and Mini-TES spectra for Cliffhanger are dominated by dust, whereas the MB data show the presence of nanophase iron oxides (a dust component) and pyroxene, i.e., MB has a greater penetration depth than either Pancam or Mini-TES and can see more of the underlying pyroxene. *Sullivan et al.* [2008] also hypothesize on the basis of the presence of angular grains (i.e., not

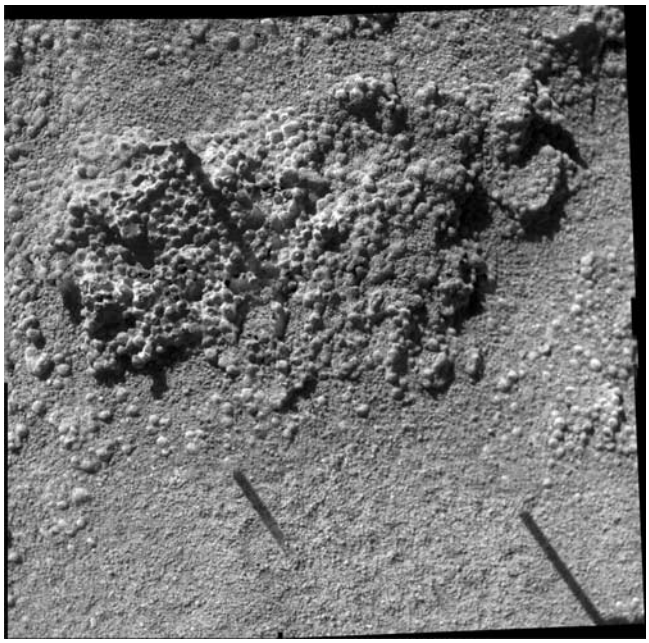

Figure 14. Microscopic Imager view of King George Island, a friable, platy deposit (see Figure 11) of round, uniformly sand sized grains. Average grain size is ~1 mm. Mosaic covers ~6 cm in width. Wind-blown soil can be seen surrounding the rock at the top and bottom of the mosaic. The composition of this outcrop is mainly SiO_2, followed in relative abundance by FeO, MgO, and Al_2O_3 (Table 6). The iron mineralogy is dominated by hematite (43%; Table 5 and Figure 15), implying alteration under oxidizing conditions to remove iron from ferromagnesian silicates to form hematite. The dark lines are MI poker shadows. Mosaic generated from frames 2M217894337IFFAS20P2956M2F1, 2M217894630IFFAS20P2956M2F1, 2M217894945IFFAS20P2956M2F1, and 2M217895270IFFAS20P2956M2F1 acquired on sol 1031.

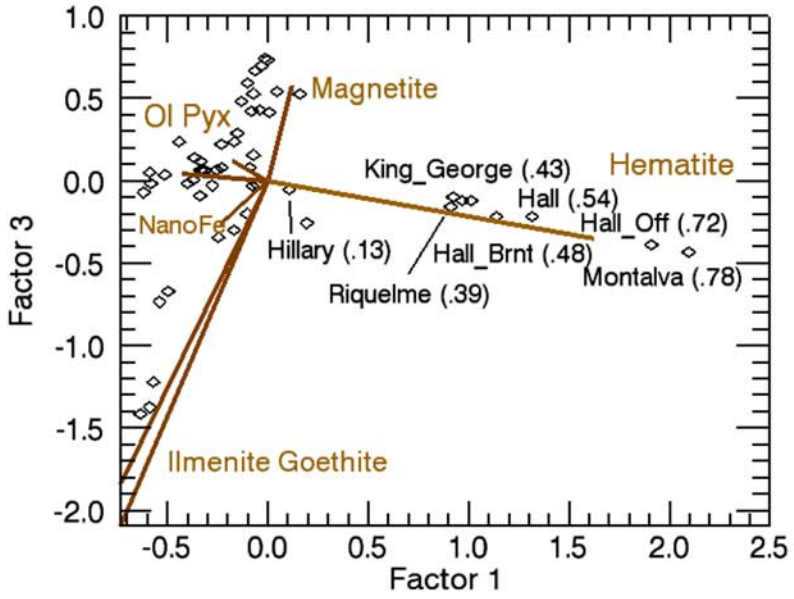

Figure 15. MB-based correspondence analysis of all rocks in the Inner Basin showing hematite enrichment for the friable, platy outcrops exposed on the floor of Eastern Valley and Low and Mitcheltree Ridges. Numbers refer to the fraction of the iron that is contained within hematite. Montalva is stratigraphically below the Riquelme Outcrop at Troll. A series of measurements were made on different sections of Halley and are shown, along with King George Island. Hillary is a rock from the summit of Husband Hill with a fairly large amount of nanophase iron oxide, magnetite, and hematite [*Morris et al.*, 2008]. Factors 1 and 3 are used because this projection shows the hematite trend better than other planes. Factors 1 and 3 capture 67% of the variance in the data set.

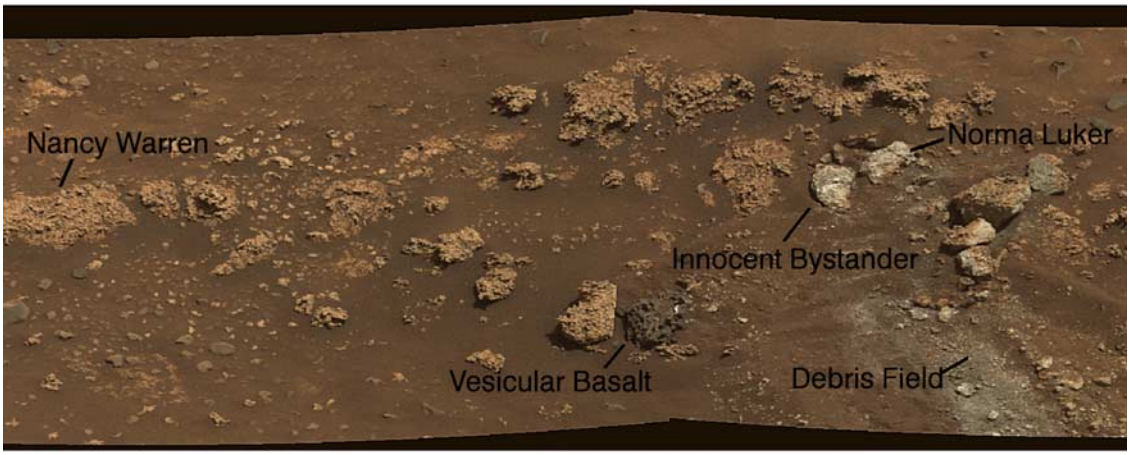

Figure 16. Pancam false color mosaic showing the Nancy Warren, Innocent Bystander, and Norma Luker targets in detail. Innocent Bystander and Norma Luker represent rocks broken apart by wiggling (using the operative azimuthal actuator) and dragging Spirit's right front wheel over them. Note the debris field produced when the rover backed up after doing its crushing. The dark rock labeled vesicular basalt is typical of numerous clasts and boulders shown to be of basaltic composition. The Pancam frames used were 2P235913627ESFAU37P2378L2M1, 2P235913690ESFAU37P2378L5M1, 2P235913733ESFAU37P2378L7M1, 2P235913941ESFAU37P2378L2M1, 2P235914094ESFAU37P2378L5M1, and 2P235914221ESFAU37P2378L7M1.

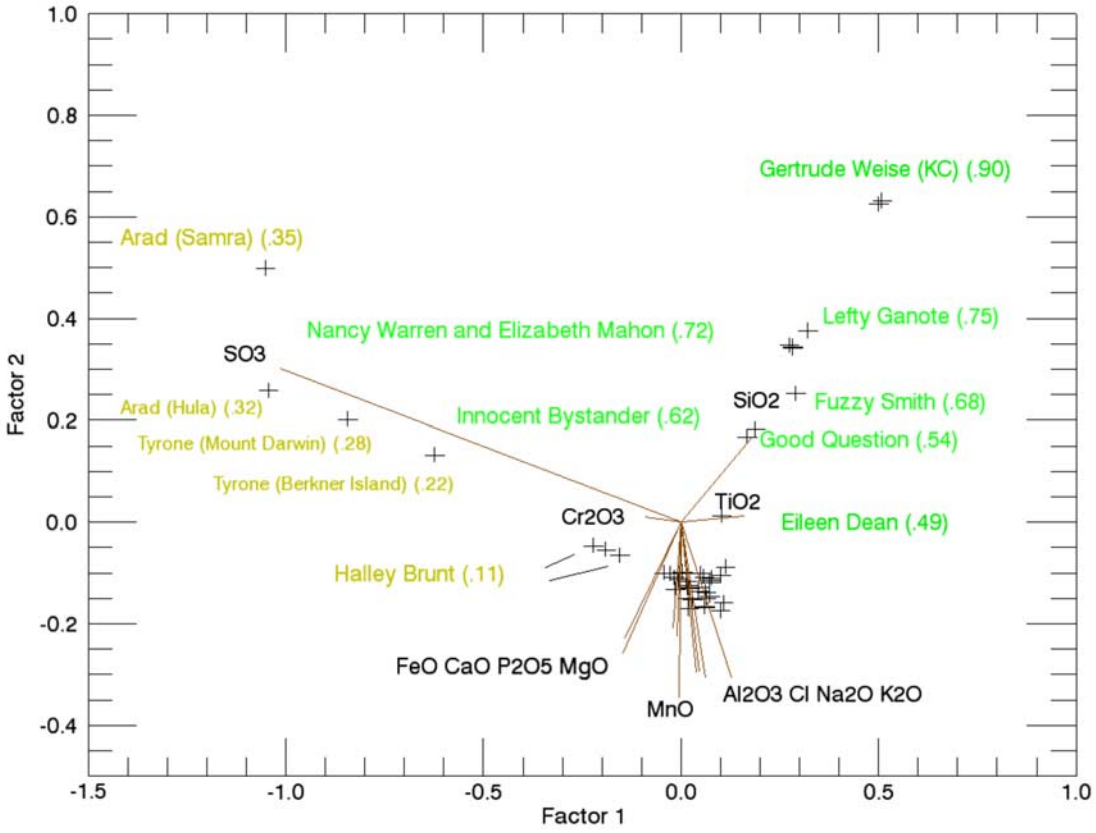

Figure 17. Factors 1 versus 2 plot from correspondence analysis applied to APXS data for Inner Basin targets. Note that the SiO_2 and SO_3 vectors plot toward the top of the diagram and that key targets follow these vectors and show progressive enrichments in both SiO_2 and SO_3, although the targets split into SiO_2- and SO_3-dominated trends. Numbers and labels in yellow are for SO_3 concentrations, whereas those in green are for SiO_2 concentrations. Arad (Samra) is the disturbed soil with the highest abundance of SO_3 (35%) and Kenosha Comets in the Gertrude Weise disturbed soil has the highest abundance of SiO_2. This projection captures 87% of the variance of the multivariate data set.

Figure 18. Color image from the Kau Desert, Hawaii, showing differentially eroded accretionary lapilli basaltic ash deposits draped over vesicular basalt flow outcrops and boulders. Rock hammer for scale.

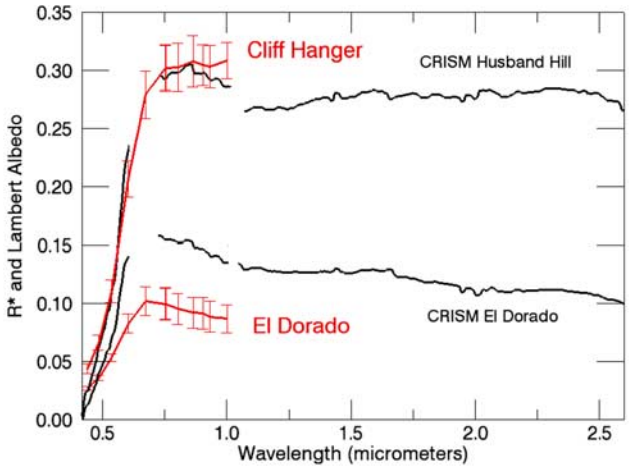

Figure 19. CRISM spectra retrieved from FRT00003192–07 for light-toned ripples on Husband Hill and Tennessee Valley and the dark El Dorado ripple field, overlain Pancam spectra retrieved for undisturbed surfaces on the Cliffhanger and El Dorado ripples. Data are shown between 0.4 and 2.5 μm only to emphasize comparisons with Pancam data, although retrievals extended to 4.0 μm. The spectral data are consistent with control by iron-bearing minerals, with strong ferric absorption edges shortward of 0.8 μm, broad absorptions between 0.8 and 1.5 μm due to olivine and pyroxene, and a negative slope longward of 0.8 μm for the El Dorado spectrum due to a thin dust cover that becomes translucent at long wavelengths to reveal the underlying mafic sand signature. The upturn for the longest Pancam wavelength for the Cliffhanger ripple is interpreted to be a consequence of a large dust component for this surface ($\sim$10 cm wide patch) as compared to the CRISM data (3 $\times$ 3 pixel averages at 18 m/pixel) for the two spectra. Gap in CRISM data $\sim$0.7 μm is a nonrecoverable portion of the spectrum where two detectors join. Gap just longward of 1 μm is the join between the *S* and *L* CRISM detectors [*Murchie et al.*, 2007]. Pancam spectra extracted from scenes quoted in Figure 7 caption.

rounded by extensive erosion and transport) that the Cliffhanger ripples contain a significant contribution from local outcrops in Tennessee Valley. In fact, correspondence analysis applied to elemental abundances determined for soils by Spirit shows that the Cliffhanger ripples have a chemical affinity for Wishstone rocks (Figure 23). As noted in section 3 of this paper, Wishstone materials dominate the rock population on Husband Hill on the basis of Mini-TES spectra. Wishstone (and Watchtower, its altered equivalent [*Ming et al.*, 2008]) will add feldspar (Figure 9, from Mini-TES data) to the light-toned ripples in the Tennessee Valley and the northwestern side of the Husband Hill summit. Feldspar would be spectrally neutral and thus not uniquely detectable in the Pancam and CRISM wavelength intervals. Thus, the orbital and surface observations combined provide a self-consistent picture of what is controlling the spectral variety at the 18 m/pixel scale relevant to the CRISM measurements, i.e., regional-scale aeolian mixing of dust and sand with local materials.

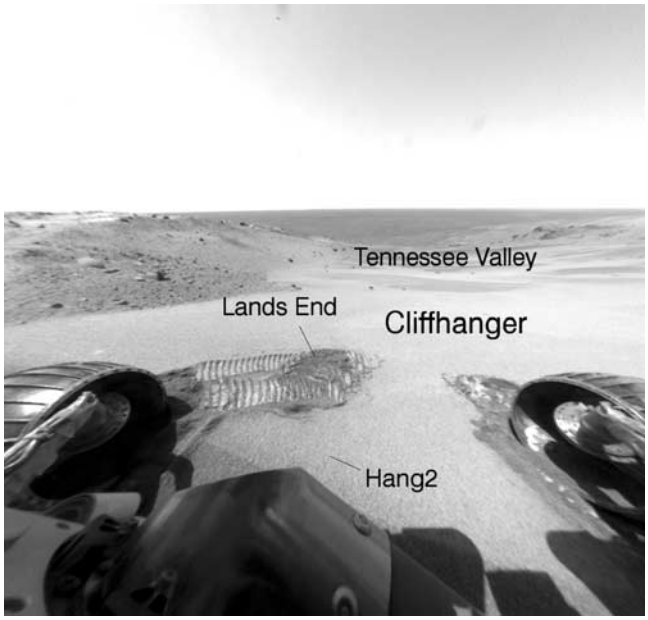

Figure 20. Hazcam frame covering Cliffhanger ripple scuff experiments on the summit of Husband Hill. Hang2 is the location for the MB and APXS undisturbed surface measurements. View is looking toward the northwest into the Tennessee Valley and shows the set of light-toned ripples that have migrated toward the summit. Frame 2F180078494RSLAEM9P1214L0MZ acquired on sol 605.

[33] Examination of CRISM spectra for the Columbia Hills shows a smooth variation in albedo and shape consistent with mixing between the end-members described in the last paragraphs and shown in Figure 19. This is not

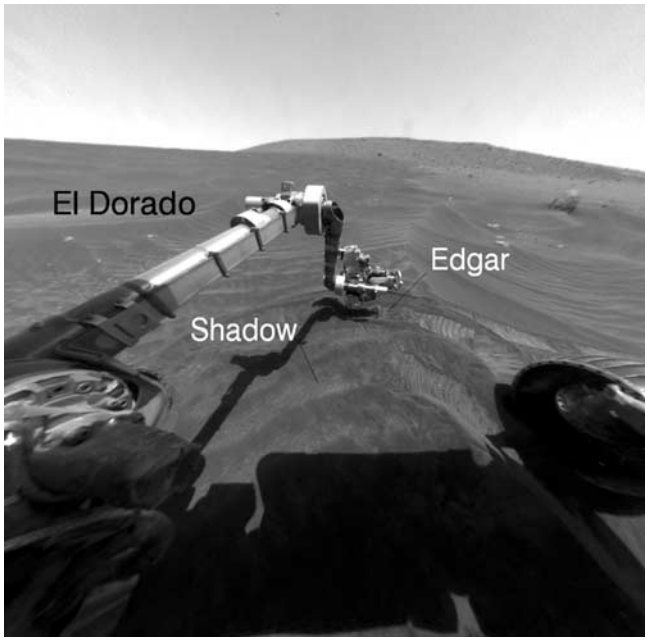

Figure 21. Hazcam frame covering El Dorado scuff experiments and looking back toward Husband Hill. Shadow is the location for the MB undisturbed surface measurements. Frame 2F189393623RSLAL00P1121L0MZ acquired on sol 710.

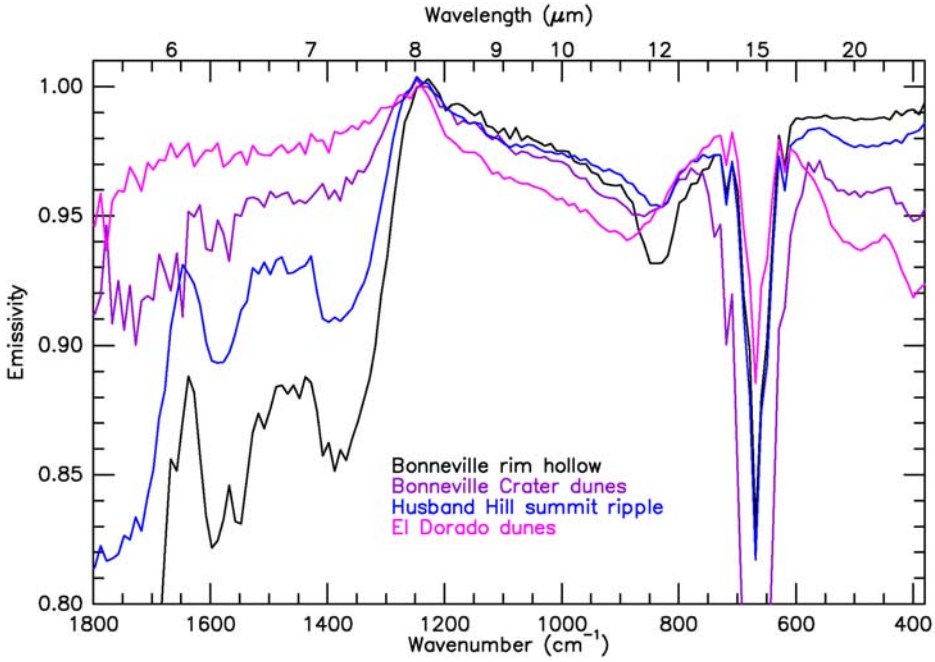

Figure 22. Mini-TES spectra are shown for Cliffhanger and El Dorado ripple surfaces, together with spectra from a visually bright and dusty hollow on the rim of Bonneville Crater (Figure 1) and dark ripples within that crater. The dark ripple fields have spectra controlled by olivine (particularly the long-wavelength region, compare to Figure 9 for Adirondack). The light-toned ripple surfaces are dominated by dust signatures.

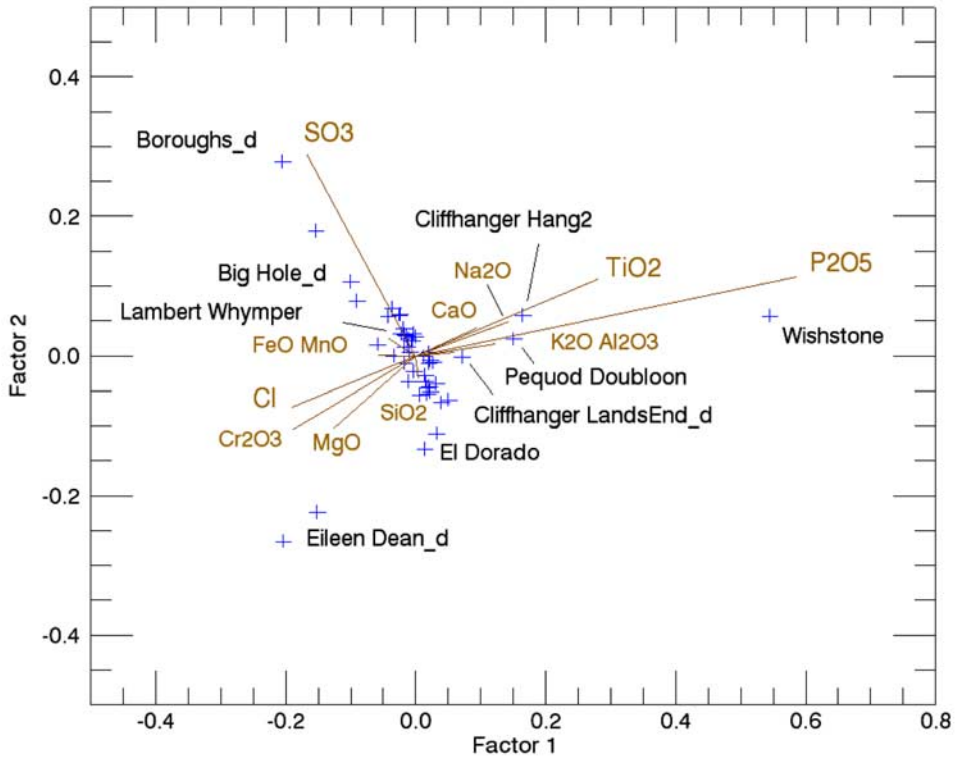

Figure 23. APXS-based correspondence analysis for all soils examined by Spirit. The Wishstone float rock analysis is also shown. The appended "_d" means that the soil has been disturbed or excavated by Spirit's wheels. The range of natural soil surfaces varies from El Dorado (basaltic sand, with both disturbed and undisturbed samples shown) to Lambert Whymper (basaltic sand and dust). Eileen Dean is located at an extreme position because of its abundance of Cr_2O_3 and MgO and as noted in the text has been altered. Cliffhanger and Pequod Doubloon are soils that have the addition of local Wishstone materials. Boroughs and Big Hole are subsurface trench soil analyses showing an enrichment in SO_3. Data from *Gellert et al.* [2006] and *Ming et al.* [2008]. Captures 78% of the variance of the data set.

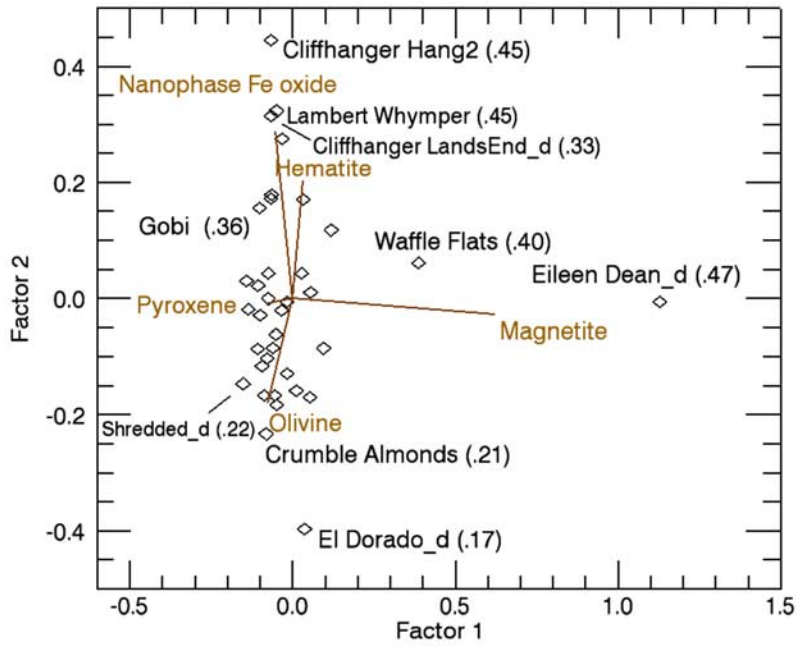

Figure 24. MB-based correspondence analysis showing trends from basaltic sand with a small amount of dust indicated by high abundance of olivine, pyroxene, and magnetite (e.g., El Dorado ripple field) to basaltic sand with a significant amount of dust delineated by nanophase iron oxides, e.g., Cliffhanger Hang2 on the Cliffhanger light-toned ripple field. Numbers represent Fe^{+3}/Fe_{total} ratios. Chromite has not been included in the correspondence analysis since this mineral was only found in the Assemblee rock [*Morris et al.*, 2008]. The _d for soils refers to scuffed soils or soils disturbed by Spirit's wheels during drives. Cliffhanger Hang2 is the undisturbed surface for Cliffhanger, whereas Cliffhanger LandsEnd_d corresponds to the measurement within the scuff zone. Eileen Dean is a highly altered soil exposed by the rover's wheels, as noted in the text. The factors 1 versus 2 plane projection accounts for 78% of the multidimensional data set variance.

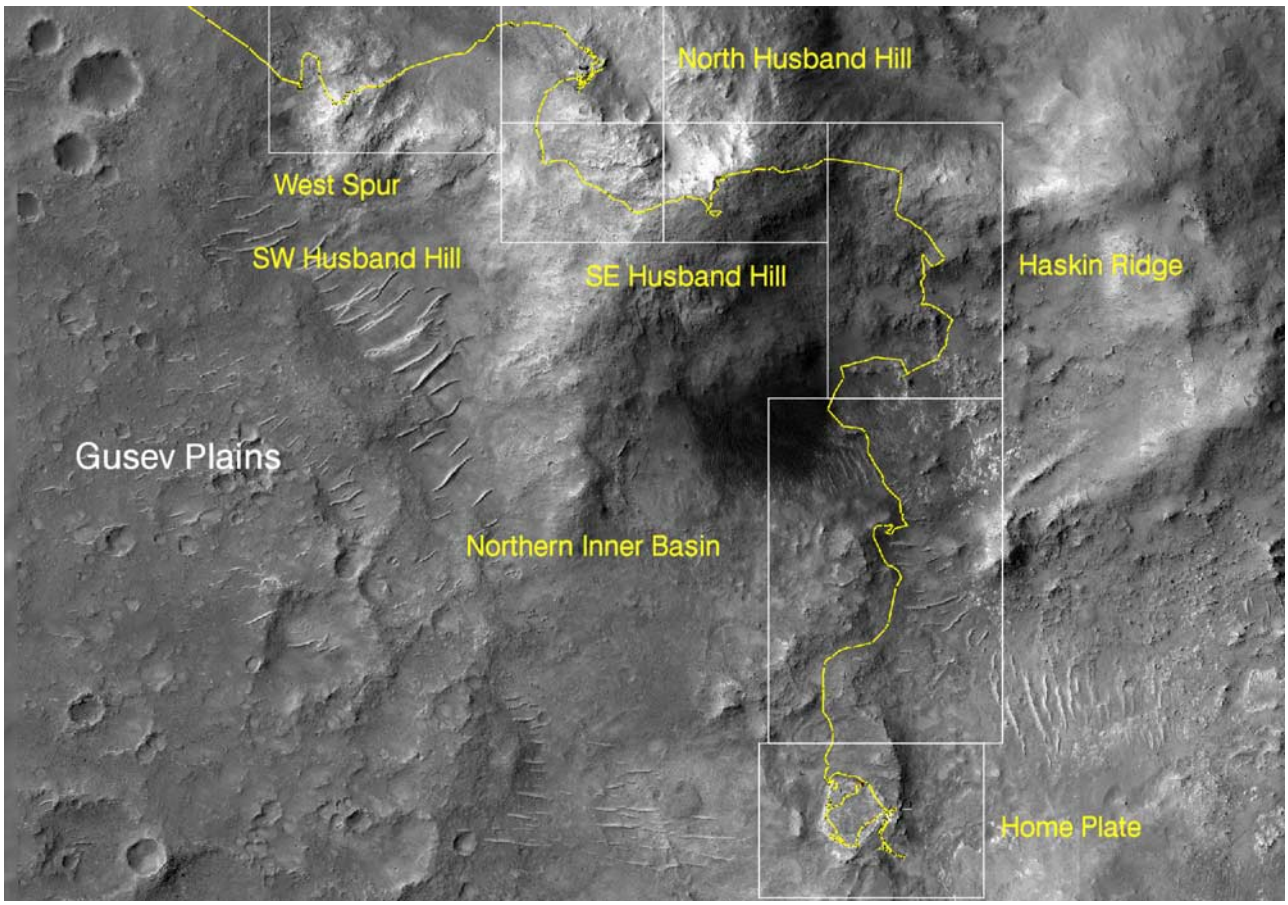

Figure A1. Overview of Spirit's traverses. Image covers ~1900 m in width.

surprising considering that Spirit has mainly encountered wind-blown soils on West Spur, Husband Hill, and the Inner Basin, i.e., the mineralogical variations and aqueous alteration associated with the various rock types encountered by Spirit are not evident because the rock areal footprint is small relative to soil and dust covers. A spectral dominance by iron bearing minerals is also evident when comparing the patterns for MB observations for soils examined by Spirit to the end-members found in the CRISM spectra (Figures 19 and 24). The Cliffhanger undisturbed surface MB observation (Hang2) has the highest ratio of Fe^{+3}/Fe_{total} (0.45) and the highest abundance of nanophase iron oxides of any soil (including the plains soils) whereas El Dorado (0.17) has the lowest ratio and highest proportion of olivine and pyroxene (Table 5). The vast majority of soils fall on a mixing line between El Dorado and Hang2 with olivine and pyroxene dominating the former and nanophase iron oxide in much higher abundance in the latter. Magnetite pulls the soil data off a simple mixing line, as expected, with an extreme case defined by the disturbed soil, Eileen Dean, found close to Nancy Warren (Figure 16). But, this material would not be evident from orbit because it was found in one of Spirit's wheel tracks. Eileen Dean, with its unusually high concentration of magnetite, MgO, Cr_2O_3, Zn, Ni, and Cl, unusually low NaO and Al_2O_3, and the presence in Mini-TES of a ~6 μm water bending mode vibration, is unusual in many respects and probably represents yet another type of aqueous alteration not observable from orbit because of the ubiquitous cover of wind-blown sand [*Morris et al.*, 2008; *Ming et al.*, 2008].

6. Conclusions and Implications

[34] Spirit has shown extensive evidence for interaction of water and crustal materials over its ~1500 sols of exploration. This includes Voltaire, altered impact or volcanic rocks on Husband Hill, and the formation of volcaniclastic materials with hematite, sulfate, and opaline silica enrichment produced by aqueous processes in and around Home Plate in the Inner Basin. On the other hand, orbital spectral observations by the CRISM hyperspectral imager (0.4–4.0 μm) are dominated by the presence of iron-bearing phases. The discrepancy between extensive evidence for aqueous alteration discovered by Spirit and the dominance of iron-bearing minerals from orbit is resolved when it is realized that windblown deposits dominate the traverse sites by areal extent and that the evidence for alteration observed by Spirit occur in outcrops that are too small and/or mostly buried to be resolved in the 18 m/pixel orbital data. OMEGA and CRISM observations show the presence of phyllosilicates, hydrated sulfates, and opaline silica elsewhere on Mars where these deposits are exposed on spatial length scales properly sampled by the spatial footprints for these sensors. The fact that the Columbia Hills shows evidence for extensive aqueous alteration when examined in detail over much smaller length scales (i.e., from Spirit)

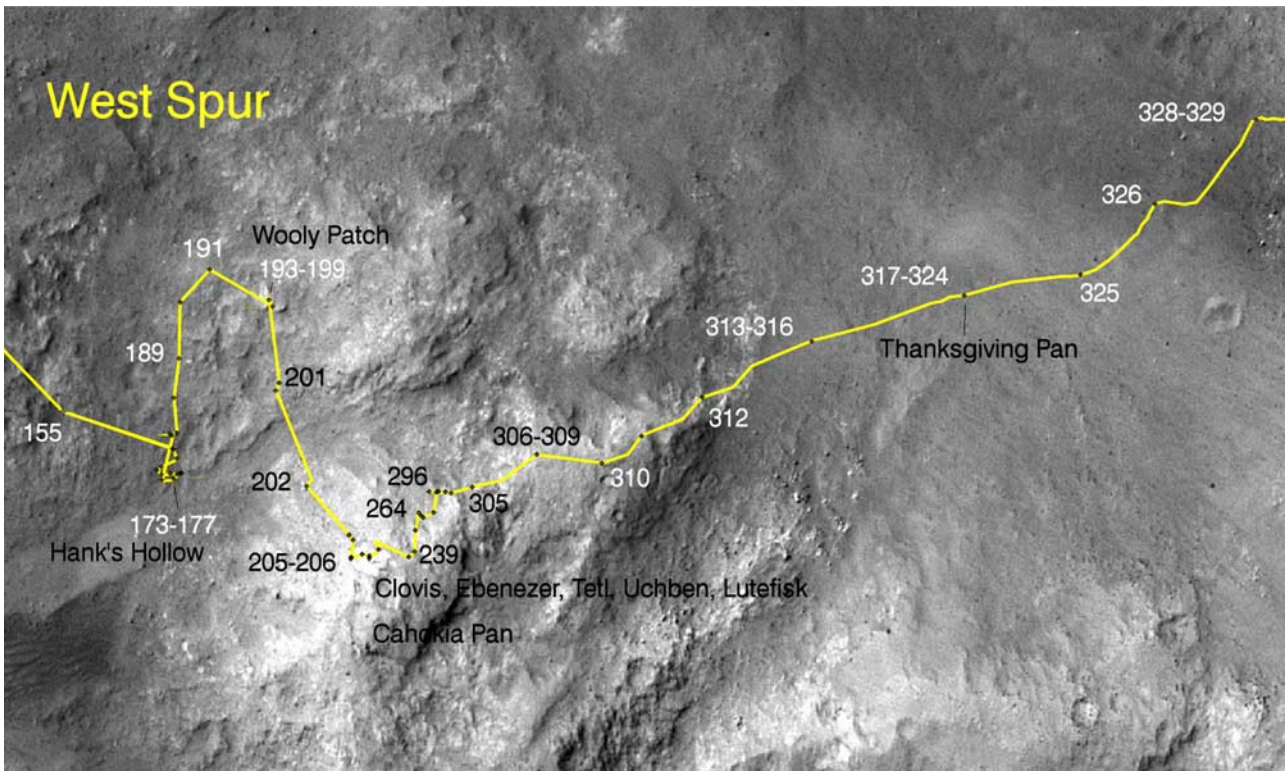

Figure A2. Traverses are shown across West Spur.

bodes well for continued and detailed observations by future rover missions that are focused on "following the water" and evaluating whether or not the planet was once habitable. We suggest that older terrains on Mars are likely to have been ubiquitously altered by aqueous processes, increasing the likelihood that the planet was once habitable and that the evidence has been preserved.

Appendix A

[35] In this Appendix we provide detailed traverse information for Spirit, overlain on HiRISE image PSP_001513_1655_red, projected to an equirectangular map base. To precisely locate the rover on any given sol the ensemble of rover observations was used by us to locate the position on the HiRISE image using a combination of nearby and horizon landmarks. The locations were cross-checked against a bundle-adjusted set of locations derived from stereo image analysis by *Li et al.* [2008]. The presentation includes an overview map (Figure A1) showing the traverses, together with boxes that show enlargements in Figures A2–A8. Sols, sites, and key terrain features are shown on the enlargements, although the high density of experiment sites in Eastern Valley

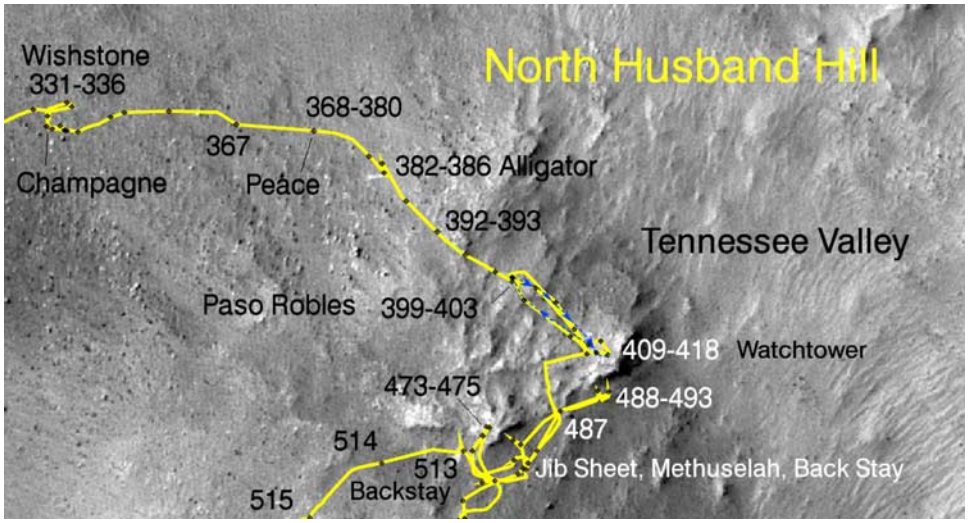

Figure A3. Traverses are shown across the northern portion of Spirit's travels on Husband Hill.

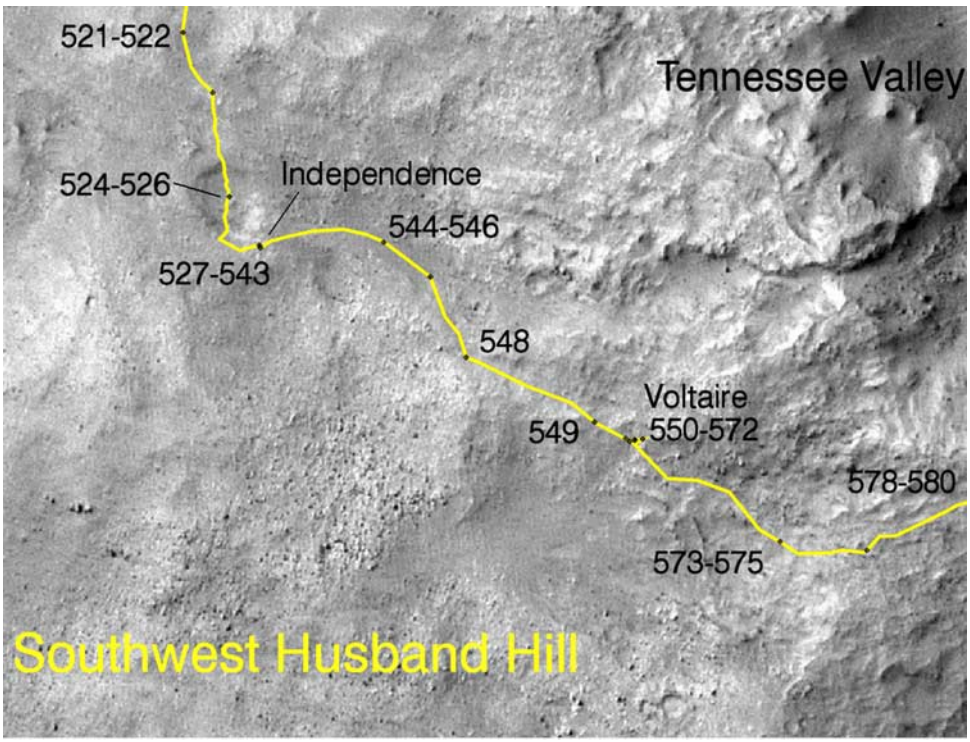

Figure A4. Traverses are shown across the southwestern portion of Spirit's travels on Husband Hill.

(Figure A8) precludes delineation of each location. These overlays should be used in combination with Tables 2 and 3, Figure 3, and the description of operations provided in the main body of the paper to understand what Spirit has accomplished. Note that the box labels refer to relative locations of the boxes on Husband Hill and not to absolute cardinal positions. The detailed traverses and measurements conducted in Eastern valley are not possible to show in detail on a HiRISE base map.

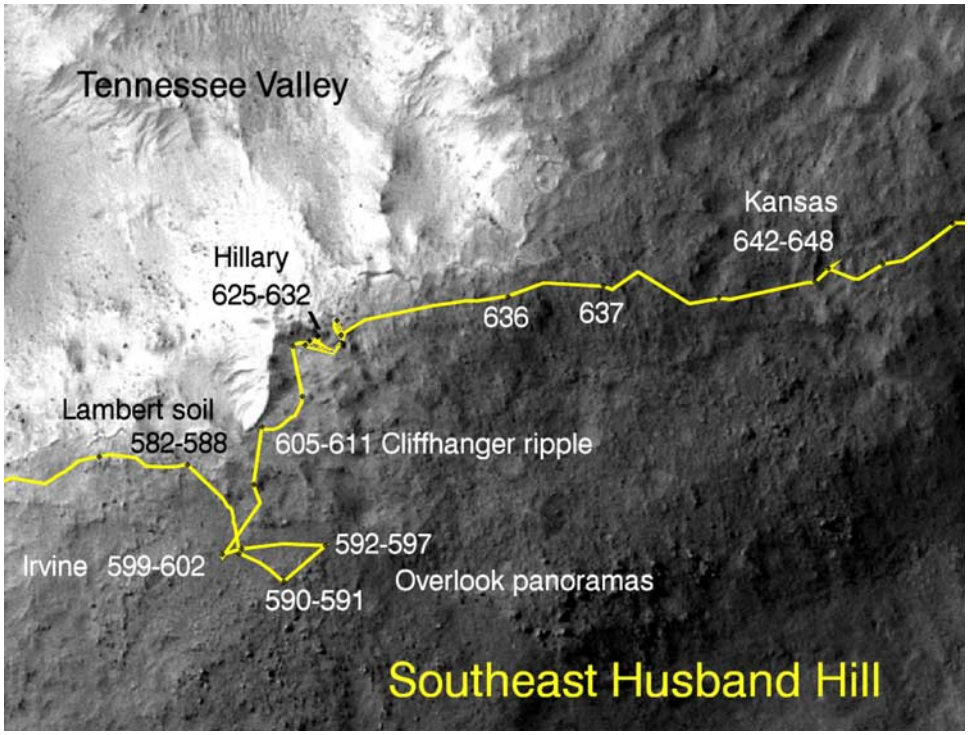

Figure A5. Traverses are shown across the southeastern portion of Spirit's travels on Husband Hill.

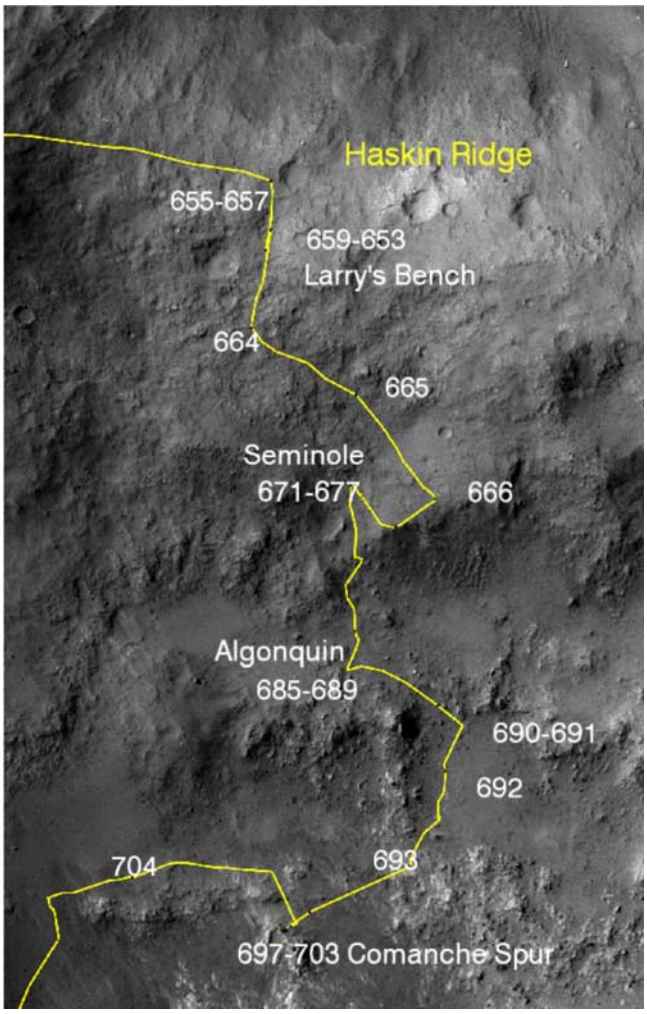

Figure A6. Spirit's traverses are shown across the Haskin Ridge and areas to the south.

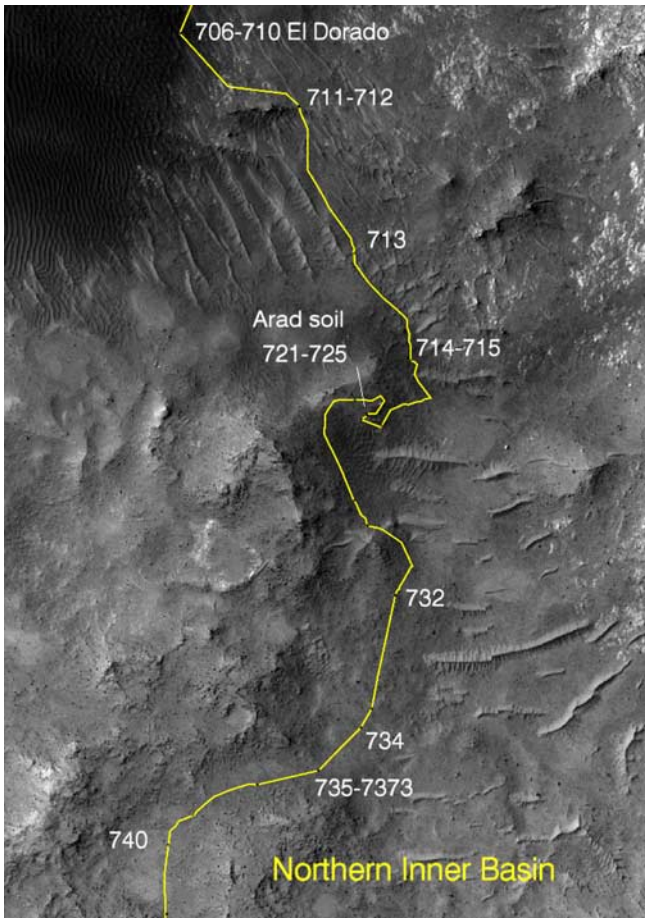

Figure A7. Spirit's traverses are shown across a portion of the El Dorado area and the northern portion of the Inner Basin.

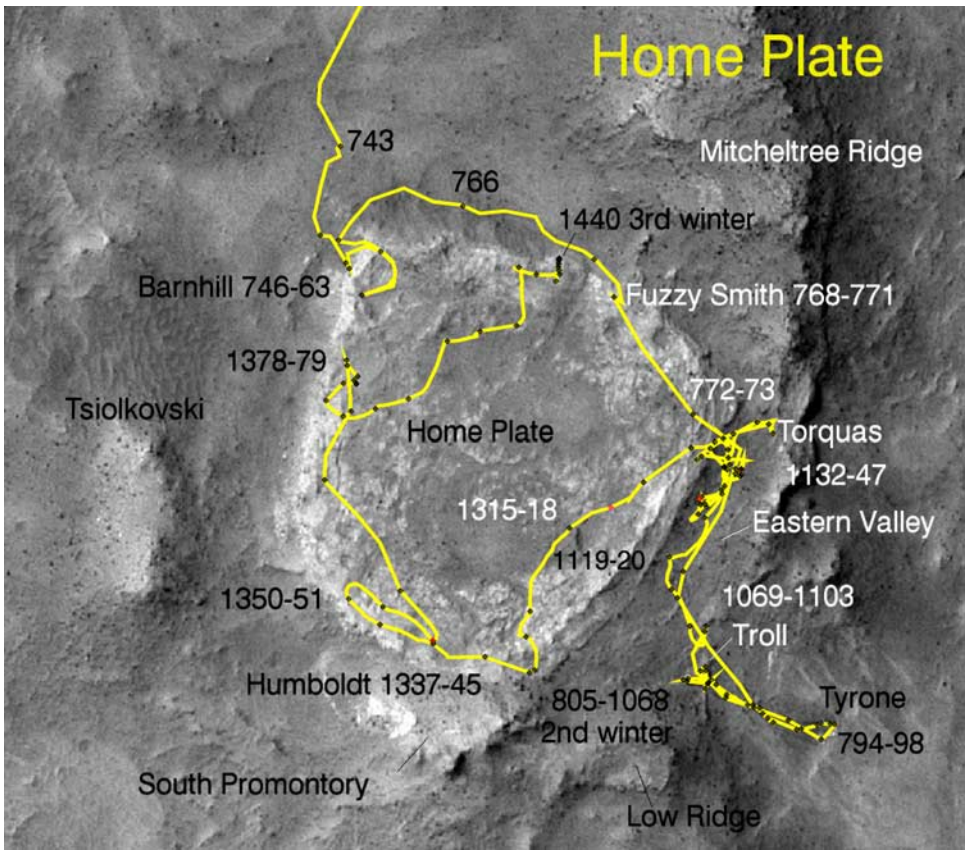

Figure A8. Spirit's traverses are shown across Home Plate and surrounding areas.

[36] **Acknowledgments.** We thank the capable team of engineers and scientists who made the Spirit mission possible, and we thank NASA for its support of our endeavors and the HiRISE, CTX, and CRISM teams who worked to acquire, process, and release the orbital data used in this study. We also thank Bethany Ehlmann and Horton Newsom for thoughtful reviews. C. S. specifically acknowledges support by an appointment to the NASA Postdoctoral Program at the Johnson Space Center, administered by Oak Ridge Associated Universities through a contract with NASA.

References

Arvidson, R. E., F. Poulet, J.-P. Bibring, M. Wolff, A. Gendrin, R. V. Morris, J. J. Freeman, Y. Langevin, N. Mangold, and G. Bellucci (2005), Spectral reflectance and morphologic correlations in eastern Terra Meridiani, Mars, *Science*, *307*(5715), 1591–1594, doi:10.1126/science.1109509.

Arvidson, R. E., et al. (2006a), Overview of the Spirit Mars Exploration Rover Mission to Gusev Crater: Landing site to Backstay Rock in the Columbia Hills, *J. Geophys. Res.*, *111*, E02S01, doi:10.1029/2005JE002499.

Arvidson, R. E., et al. (2006b), Nature and origin of the hematite-bearing plains of Terra Meridiani based on analysis of orbital and Mars Exploration Rover data sets, *J. Geophys. Res.*, *111*, E12S08, doi:10.1029/2006JE002728.

Burns, R. (1993), Origin of electronic spectra of minerals in the visible to near-infrared region, in *Remote Geochemical Analysis: Elemental and Mineralogical Composition*, edited by C. Pieters and P. Englert, pp. 3–29, Cambridge Univ. Press, New York.

Clark, B. C., et al. (2007), Evidence for montmorillonite or its compositional equivalent in Columbia Hills, Mars, *J. Geophys. Res.*, *112*, E06S01, doi:10.1029/2006JE002756.

Farrand, W. H., J. F. Bell III, J. R. Johnson, S. W. Squyres, J. Soderblom, and D. W. Ming (2006), Spectral variability among rocks in visible and near infrared multispectral Pancam data collected at Gusev Crater: Examinations using spectral mixture analysis and related techniques, *J. Geophys. Res.*, *111*, E02S15, doi:10.1029/2005JE002495.

Fischer, E. M., and C. M. Pieters (1993), The continuum slope of Mars: Bidirectional reflectance investigations and applications to Olympus Mons, *Icarus*, *102*, 185–202, doi:10.1006/icar.1993.1043.

Gellert, R., et al. (2006), Alpha Particle X-Ray Spectrometer (APXS): Results from Gusev crater and calibration report, *J. Geophys. Res.*, *111*, E02S05, doi:10.1029/2005JE002555.

Gendrin, A., et al. (2005), Sulfates in Martian layered terrains: The OMEGA/Mars express view, *Science*, *307*(5715), 1587–1591, doi:10.1126/science.1109087.

Haskin, L. A., et al. (2005), Water alteration of rocks and soils on Mars at the Spirit rover site in Gusev Crater, *Nat.*, *436*, 66–69, doi:10.1038/nature03640.

Johnson, J. R., and W. M. Grundy (2001), Visible/near-infrared spectra and two-layer modeling of palagonite-coated basalts, *Geophys. Res. Lett.*, *28*, 2101–2104, doi:10.1029/2000GL012669.

Johnson, J. R., J. F. Bell III, E. Cloutis, M. Staid, W. H. Farrand, T. McCoy, M. Rice, A. Wang, and A. Yen (2007), Mineralogic constraints on sulfur-rich soils from Pancam spectra at Gusev crater, Mars, *Geophys. Res. Lett.*, *34*, L13202, doi:10.1029/2007GL029894.

Kurtz, A. C., L. A. Derry, and O. A. Chadwick (2002), Germanium-silicon fractionation in the weathering environment, *Geochem. Cosmochim. Acta*, *66*, 1525–1537.

Lewis, K., O. Aharonson, and M. Schmidt (2007), Stratigraphy and structure of Inner Basin outcrops in the Columbia Hills from the Spirit rover, paper presented at 38th Lunar and Planetary Science Conference, Lunar and Planet. Inst., League City, Tex.

Lewis, K. W., O. Aharonson, J. P. Grotzinger, S. W. Squyres, and M. E. Schmidt (2008), Structure and stratigraphy of Home Plate from the Spirit Mars Exploration Rover, *J. Geophys. Res.*, doi:10.1029/2007JE003025, in press.

Li, R., et al. (2008), Characterization of traverse slippage experienced by Spirit rover on Husband Hill at Gusev Crater, *J. Geophys. Res.*, doi:10.1029/2008JE003097, in press.

Lichtenberg, K. A., et al. (2007), Coordinated analyses of orbital and Spirit Rover data to characterize surface materials on the cratered plains of Gusev Crater, Mars, *J. Geophys. Res.*, *112*, E12S90, doi:10.1029/2006JE002850.

Madsen, M. B., et al. (2008), Overview of the Magnetic Properties Experiments on the Mars Exploration Rovers, *J. Geophys. Res.*, doi:10.1029/2008JE003098, in press.

Malin, M. C., D. Dzurisin, and R. P. Sharp (1983), Stripping of Keanakakoi tephra on Kilauea Volcano, Hawaii, *Geol. Soc. Am. Bull.*, *94*, 1148–1158, doi:10.1130/0016-7606(1983)94<1148:SOKTOK>2.0.CO;2.

Malin, M. C., et al. (2007), Context camera investigation on board the Mars Reconnaissance Orbiter, *J. Geophys. Res.*, *112*, E05S04, doi:10.1029/2006JE002808.

Martinez-Alonso, S., B. M. Jakosky, M. T. Mellon, and N. E. Putzig (2005), A volcanic interpretation of Gusev crater surface materials from thermophysical, spectral, and morphological evidence, *J. Geophys. Res.*, *110*, E01003, doi:10.1029/2004JE002327.

McCoy, T. J., et al. (2008), Structure, stratigraphy, and origin of Husband Hill, Columbia Hills, Gusev Crater, Mars, *J. Geophys. Res.*, *113*, E06S03, doi:10.1029/2007JE003041.

McEwen, A. S., et al. (2007), Mars Reconnaissance Orbiter's High Resolution Imaging Science Experiment (HiRISE), *J. Geophys. Res.*, *112*, E05S02, doi:10.1029/2005JE002605.

McSween, H. Y., et al. (2006), Alkaline volcanic rocks from the Columbia Hills, Gusev crater, Mars, *J. Geophys. Res.*, *111*, E09S91, doi:10.1029/2006JE002698.

McSween, H. Y., et al. (2008), Mineralogy of volcanic rocks in Gusev Crater, Mars: Reconciling Mössbauer, Alpha Particle X-Ray Spectrometer, and Miniature Thermal Emission Spectrometer spectra, *J. Geophys. Res.*, *113*, E06S04, doi:10.1029/2007JE002970.

Milliken, R. E., et al. (2008), Opaline silica in young deposits on Mars, *Geology*, in press.

Ming, D. W., et al. (2006), Geochemical and mineralogical indicators for aqueous processes in the Columbia Hills of Gusev Crater, Mars, *J. Geophys. Res.*, *111*, E02S12, doi:10.1029/2005JE002560.

Ming, D. W., et al. (2008), Geochemical properties of rocks and soils in Gusev Crater, Mars: Results of the Alpha Particle X-Ray Spectrometer from Cumberland Ridge to Home Plate, *J. Geophys. Res.*, doi:10.1029/2008JE003195, in press.

Morris, R. V., et al. (2000), Mineralogy, composition, and alteration of Mars Pathfinder rocks and soils: Evidence from multispectral, elemental, and magnetic data on terrestrial analogue, SNC meteorite, and Pathfinder samples, *J. Geophys. Res.*, *105*(E1), 1757–1817, doi:10.1029/1999JE001059.

Morris, R. V., et al. (2006), Mössbauer mineralogy of rock, soil, and dust at Gusev Crater, Mars: Spirit's journey through weakly altered olivine basalt on the Plains and pervasively altered basalt in the Columbia Hills, *J. Geophys. Res.*, *111*, E02S13, doi:10.1029/2005JE002584.

Morris, R. V., et al. (2008), Iron mineralogy and aqueous alteration from Husband Hill through Home Plate at Gusev Crater, Mars, from the Mössbauer Instrument on the Spirit Mars Exploration Rover, *J. Geophys. Res.*, doi:10.1029/2008JE003201, in press.

Murchie, S. L., et al. (2007), Compact Reconnaissance Imaging Spectrometer for Mars (CRISM) on Mars Reconnaissance Orbiter (MRO), *J. Geophys. Res.*, *112*, E05S03, doi:10.1029/2006JE002682.

Mustard, J. F., et al. (2008), Hydrated silicate minerals on Mars observed by the CRISM instrument on MRO, *Nat.*, *454*, 305–309, doi:10.1038/nature07097.

Parfitt, R. L., and R. J. Furkert (1980), Identification and structure of two types of allophane from volcanic ash soils and tephra, *Clays Clay Miner.*, *28*, 328–334, doi:10.1346/CCMN.1980.0280502.

Parke, S. (1974), Glasses, in *The Infrared Spectra of Minerals*, edited by V. C. Farmer, pp. 483–514, Mineral. Soc. of G. B. and Ireland, Twickenham, U. K.

Poulet, F., J.-P. Bibring, J. F. Mustard, A. Gendrin, N. Mangold, Y. Langevin, R. E. Arvidson, B. Gondet, and C. Gomez (2005), Phyllosilicates on Mars and implications for the early Mars History, *Nat.*, *438*, 623–627, doi:10.1038/nature04274.

Rice, M., J. Bell, A. Wang, and E. Cloutis (2008), VIS-NIR spectral characterization of Si-rich deposits at Gusev Crater, Mars, paper presented at 39th Lunar and Planetary Science Conference, Lunar and Planet. Inst., League City, Tex.

Ruff, S. W., P. R. Christensen, D. L. Blaney, W. H. Farrand, J. R. Johnson, J. R. Michalski, J. E. Moersch, S. P. Wright, and S. W. Squyres (2006), The rocks of Gusev Crater as viewed by the Mini-TES instrument, *J. Geophys. Res.*, *111*(E12), E12S18, doi:10.1029/2006JE002747.

Schiffman, P., R. Zierenberg, N. Marks, J. Bishop, and M. Dyer (2006), Acid-fog deposition at Kilauea volcano: A possible mechanism for the formation of siliceous rock coatings on Mars, *Geol. Soc. Am. Bull.*, *34*, 921–924.

Schmidt, M., et al. (2008), Hydrothermal origin of halogens at Home Plate, Gusev Crater, *J. Geophys. Res.*, *113*, E06S12, doi:10.1029/2007JE003027.

Squyres, S. W., et al. (2003), Athena Mars rover science investigation, *J. Geophys. Res.*, *108*(E12), 8062, doi:10.1029/2003JE002121.

Squyres, S. W., et al. (2006), Rocks of the Columbia Hills, *J. Geophys. Res.*, *111*, E02S11, doi:10.1029/2005JE002562.

Squyres, S. W., et al. (2007), Pyroclastic activity at Home Plate in Gusev Crater, Mars, *Science*, *316*, 738–742, doi:10.1126/science.1139045.

Squyres, S. W., et al. (2008), Detection of silica-rich deposits on Mars, *Science*, *320*, 1063–1067, doi:10.1126/science.1155429.

Stamnes, K., S. Tsay, W. Wiscombe, and K. Jayaweera (1988), Numerically stable algorithm for discrete-ordinate-method radiative transfer in multiple scattering and emitting layered media, *Appl. Opt.*, *27*, 2502–2509.

Sullivan, R., R. Arvidson, J. F. Bell III, M. Golombek, R. Greeley, K. Herkenhoff, J. Johnson, S. Thompson, P. Whelley, and J. Wray (2008), Wind-driven particle mobility on Mars: Insights from MER observations at "El Dorado" and surroundings at Gusev Crater, *J. Geophys. Res.*, *113*, E06S07, doi:10.1029/2008JE003101.

Wang, A., et al. (2008), Light-toned salty soils and co-existing Si-rich species discovered by the Mars Exploration Rover Spirit in Columbia Hills, *J. Geophys. Res.*, doi:10.1029/2008JE003126, in press.

Yen, A. S., et al. (2008), Hydrothermal processes at Gusev Crater: An evaluation of Paso Robles class soils, *J. Geophys. Res.*, *113*, E06S10, doi:10.1029/2007JE002978.

R. E. Arvidson, R. Greenberger, E. A. Guinness, A. Wang, and S. Wiseman, Department of Earth and Planetary Sciences, Washington University, 1 Brookings Drive, St. Louis, MO 63130, USA. (arvidson@rsmail.wustl.edu)

J. F. Bell III, S. W. Squyres, and R. J. Sullivan, Department of Astronomy, Cornell University, 610 Space Sciences Building, Ithaca, NY 14853, USA.

N. A. Cabrol, NASA Ames/SETI Institute, Moffett Field, CA 94035, USA.

B. C. Clark, Lockheed Martin Corporation, 12999 West Deer Creek Canyon Road, Littleton, CO 80125, USA.

L. S. Crumpler, New Mexico Museum of Natural History and Science, 1801 Mountain Road NW, Albuquerque, NM 87104, USA.

W. H. Farrand, Space Science Institute, 4750 Walnut Street, Suite 205, Boulder, CO 80301, USA.

R. Gellert, Department of Physics, University of Guelph, MacNaughton Building, Gordon Street, Guelph, ON, Canada N1G 2W1.

W. Goetz, Max Planck Institute for Sonnensystemforschung, 2 Max-Planck-Strasse 2, D-37191 Katlenburg-Lindau, Germany.

J. A. Grant, Center for Earth and Planetary Studies, National Air and Space Museum, Smithsonian Institution, P.O. Box 37012, Washington, DC 20013, USA.

K. E. Herkenhoff and J. R. Johnson, U. S. Geological Survey, 2255 North Gemini Drive, Flagstaff, AZ 86001, USA.

J. A. Hurowitz and A. S. Yen, Jet Propulsion Laboratory, California Institute of Technology, 4800 Oak Grove Drive, Pasadena, CA 91109, USA.

G. Klingelhöfer, Institut für Anorganische und Analytische Chemie, Johannes Gutenberg-Universität, Duesbergweg 10-14, D-55099 Mainz, Germany.

K. W. Lewis, California Institute of Technology, 1200 East California Boulevard, Pasadena, CA 91125, USA.

R. Li and M. Schmidt, Department of Civil and Environmental Engineering and Geodetic Science, Ohio State University, 470 Hitchcock Hall, 2070 Neil Avenue, Columbus, OH 43210, USA.

M. B. Madsen, Niels Bohr Institute, University of Copenhagen, Blegdamsvej 17, DK-2100 Copenhagen, Denmark.

T. J. McCoy, Department of Mineral Sciences, Smithsonian Institution, P.O. Box 37012, Washington, DC 20013, USA.

S. M. McLennan, Department of Geosciences, State University of New York, 255 Earth and Space Sciences Building, Stony Brook, NY 11794, USA.

H. Y. McSween and J. Moersch, Department of Earth and Planetary Sciences, University of Tennessee, 306 Earth and Planetary Sciences Building, Knoxville, TN 37996, USA.

D. W. Ming, R. V. Morris, and C. Schröder, Johnson Space Center, NASA, 2101 NASA Parkway, Houston, TX 77058, USA.

S. L. Murchie, Applied Physics Laboratory, Johns Hopkins University, 11100 Johns Hopkins Road, Laurel, MD 20723, USA.

S. W. Ruff, School of Earth and Space Exploration, Arizona State University, P.O. Box 871404, Tempe, AZ 85287, USA.